Hadronic structure on the light front. VIII. Light scalar and vector mesons

Wei-Yang Liu,[*] Edward Shuryak,[†] and Ismail Zahed[‡]
Center for Nuclear Theory, Department of Physics and Astronomy, Stony Brook University, Stony Brook, New York 11794–3800, USA

(Received 3 August 2023; accepted 15 March 2024; published 29 April 2024)

We use the QCD instanton vacuum model to discuss the emergence of the light scalar and vector mesons on the light front. We take into account both the instanton and anti-instanton single and molecular interactions on the light quarks, in the form of nonlocal effective interactions. Although the molecular induced interactions are suppressed by a power of the packing fraction, they are still sufficient to bind the vector mesons, while keeping most of the scalar spectrum relatively unchanged. We explicitly derive the light front distribution amplitudes and partonic functions for the scalar and vector mesons, and compare them after pertinent QCD evolution, to the available empirical and lattice measured counterparts. The Dirac electric form factors for both the pion and ρ meson are derived, and shown to compare well with current data.

DOI: 10.1103/PhysRevD.109.074029

I. INTRODUCTION

Parton distribution functions (PDFs) are used to assess most processes at high energy, whenever factorization holds. They are important for the description of inclusive and exclusive processes alike, and play an essential role in precision measurements at the current Large Hadron Collider (LHC).

The PDFs capture the longitudinal distribution of partons (quarks and gluons) in a given hadron in the light front frame, at a given resolution. These unimodular distributions are inherently nonperturbative and lightlike. The leading twist PDFs are currently accessible from experiments through pertinent parametrizations [1], or using lattice simulations following the Large Momentum Effective Field Theory (LaMET) procedure [2,3] or some variations [4,5].

The determination of the PDFs, whether empirically or through numerical simulations, does not provide a comprehensive understanding of their content for physicists, nor on the basic mechanism(s) at the origin of their composition. For that, an understanding of the QCD vacuum at some preferably low resolution is required.

At low resolution, detailed cooled lattice configurations show that the QCD vacuum is populated by instantons and anti-instantons [6]. Their effects in the formation of both the scalar and vector mesons on the light front will be the main subject of this paper. Some essential aspects of this vacuum are captured by the instanton vacuum model, which allows for a semiclassical description based on a drastically reduced set of gauge configurations [7–11].

However, the QCD instanton vacuum is inherently spacelike and is more naturally formukated in Euclidean space. In a recent series of work [12–16], two of us have shown that some of the nonperturbative aspects of the QCD instanton vacuum can be exported to the light front via an analytical continuation not in the fields but in the boost parameter. The results are a variety of central and spin-dependent potentials on the light front that provide for the emergence of a nonperturbative constituent quark type model. Similar approaches more rooted in phenomenology have been also suggested in [5,17–37].

On the light front, hadrons at low resolution are described by their lowest constituent quark and gluon Fock components. The underlying nonperturbative gluonic content is mostly packaged in the emerging constituent mass and effective interactions between the constituents, following mostly from the spontaneous breaking of chiral symmetry [12–16]. However, the description of the emerging Goldstone modes (pions and kaons) requires special care on the light front, but otherwise parallels the description in the rest frame [13,38].

Another important subtlety of the light front formulation is the apparent breaking of SO(1,3) to SO(1,2), following from the use of the infinite momentum frame. We will

[*]wei-yang.liu@stonybrook.edu
[†]edward.shuryak@stonybrook.edu
[‡]ismail.zahed@stonybrook.edu

address this issue analyzing the formation of the low-lying vector mesons in the QCD instanton vacuum. On the light front, the longitudinal and transverse vector mesons follow from different constitutive equations, with apparently different characteristics. The purpose of this work is twofold: first, we will follow up on our suggestion in [12], that the light vector mesons in the QCD instanton vacuum receive sizable contributions from the instanton-anti-instanton molecular configurations; second, we will explicitly show that despite the explicit breaking of Lorentz symmetry on the light front, the rest frame SO(1,3) symmetric vector spectra and decay constants are recovered dynamically. For completeness, we note that a number of phenomenological studies of the light mesons have been carried by many using the covariant formulation in [39–44], relativistic equal-time formulation in [45–48], and variants of the light cone formulation in [36,49–53].

The organization of the paper is as follows. In Sec. II we briefly review the emergent 't Hooft nonlocal fermionic interactions in the two-flavor QCD instanton vacuum, induced by both the single instantons and anti-instantons, and the instanton-anti-instanton molecules. The latter are chirality preserving and contribute in leading order in the vector channels. In Sec. III we show how these emerging interactions yield to the spontaneous breaking of chiral symmetry, and a running constituent quark mass. In Sec. IV we construct the pertinent light front Hamiltonian using the bookkeeping in $1/N_c$ and the diluteness of the QCD instanton vacuum. The bound states equations in the scalar and vector channels are made explicit and solved. We also show how these solutions are related to covariant formulations. In Sec. V, all scalar and vector light front wave functions in the QCD instanton vacuum with nonlocal interactions are detailed. In Sec. VI we derive the parton distribution functions for the scalar and vector mesons, and analyze their partonic content both for the unpolarized and polarized states. In Sec. VII the meson distribution amplitudes are discussed, and the results compared to existing empirical measurements and current lattice simulations. In Sec. VIII we use the light front wave functions, to derive the electromagnetic form factors for the pion and ρ and ω mesons. The results are compared to the available measurements and lattice results. Our conclusions are in Sec. IX. A number of Appendixes are included to complement some of the derivations.

II. GENERALIZED 'T HOOFT INDUCED INTERACTIONS

The QCD vacuum at low resolution is populated by mostly topologically active instantons and anti-instantons, Euclidean tunneling configurations between vacua with different topological charges [11] (and references therein). Light quarks scattering through these topological configurations develop zero modes with fixed handedness. For instance, a massless left-handed quark tunneling through an instanton can emerge as a right-handed massless quark, with the handedness flipped through an anti-instanton.

For a single quark species, this mechanism is at the origin of the explicit breaking of $\mathrm{U}_A(1)$ symmetry. For many light quark species this mechanism can account for the dual breaking of the $\mathrm{U}_A(1)$ (explicitly) and chiral symmetry (spontaneously). This is manifested through the emergent multiflavored interactions, between the light quarks zero modes.

A. Local approximation

In the noninteracting instanton vacuum, these multiflavored interactions are the well-known 't Hooft determinantal interactions. In the local approximation where the instanton size is taking to zero, the induced interactions from single instantons plus anti-instantons give

$$\mathcal{L}_I = \frac{G_I}{8(N_c^2-1)}\left\{\frac{2N_c-1}{2N_c}[(\bar\psi\psi)^2-(\bar\psi\tau^a\psi)^2-(\bar\psi i\gamma^5\psi)^2 + (\bar\psi i\gamma^5\tau^a\psi)^2]+\frac{1}{4N_c}\left[(\bar\psi\sigma_{\mu\nu}\psi)^2-(\bar\psi\sigma_{\mu\nu}\tau^a\psi)^2\right]\right\} \quad (1)$$

which are seen to mix LR chiralities. The effective coupling

$$G_I = \int d\rho n(\rho)\rho^{N_f}(2\pi\rho)^{2N_f} = \frac{n_{I+\bar I}}{2}(4\pi^2\rho^3)^{N_f}\left(\frac{1}{m^*\rho}\right)^{N_f} \quad (2)$$

is fixed by the mean-instanton density

$$\frac{n_{I+\bar I}}{2} = \int d\rho n(\rho)\prod_{f=1}^{N_f}(m_f^*\rho) \quad (3)$$

with m_f^* the induced determinantal mass [54]. At low resolution, the instanton distribution is sharply peaked around the average instanton size $\rho \approx 0.31$ fm, with a mean density $n_{I+\bar I} \sim 1$ fm^{-4}.

In the interacting instanton vacuum, additional multiflavor interactions are expected. Given the diluteness of the tunneling processes in the QCD vacuum at low resolution, the natural interactions are molecular in the form of binary instanton-anti-instanton configurations. When maximally locked in color, they induce flavor mixing interactions of the form [55]

$$\mathcal{L}_{I\bar{I}} = G_{I\bar{I}}\Big\{\frac{1}{N_c(N_c-1)}[(\bar{\psi}\gamma^\mu\psi)^2+(\bar{\psi}\gamma^\mu\gamma^5\psi)^2]-\frac{N_c-2}{N_c(N_c^2-1)}[(\bar{\psi}\gamma^\mu\psi)^2-(\bar{\psi}\gamma^\mu\gamma^5\psi)^2]$$
$$+\frac{2N_c-1}{N_c(N_c^2-1)}[(\bar{\psi}\psi)^2+(\bar{\psi}\tau^a\psi)^2+(\bar{\psi}i\gamma^5\psi)^2+(\bar{\psi}i\gamma^5\tau^a\psi)^2]$$
$$-\frac{1}{2N_c(N_c-1)}[(\bar{\psi}\gamma^\mu\psi)^2+(\bar{\psi}\tau^a\gamma^\mu\psi)^2+(\bar{\psi}\gamma^\mu\gamma^5\psi)^2+(\bar{\psi}\tau^a\gamma^\mu\gamma^5\psi)^2]\Big\} \tag{4}$$

which are LL and RR chirality preserving, in contrast to (1). The effective molecule-induced coupling is defined as

$$G_{I\bar{I}} = \int d\rho_I d\rho_{\bar{I}} \int dud^4R \frac{1}{8T_{I\bar{I}}^2}(4\pi^2\rho_I^2)(4\pi^2\rho_{\bar{I}}^2)n(\rho_I)n(\rho_{\bar{I}})T_{I\bar{I}}(u,R)^{2N_f}\rho_I^{N_f}\rho_{\bar{I}}^{N_f}. \tag{5}$$

Here $R = z_I - z_{\bar{I}}$ is the relative molecular separation, $u_\mu = \frac{1}{2i}\mathrm{tr}(U_{\bar{I}}\tau_\mu^+ U_I^\dagger)$ is the relative molecular orientation with the locked color with $\tau_\mu^+ = (\vec{\tau}, -i)$, and $T_{I\bar{I}}$ is the hopping quark matrix. Equation (5) is readily understood as the unquenched tunneling density for a molecular configuration, whereby a pair of quark lines is removed by the division $T_{I\bar{I}}^2$ to account for the induced four-Fermi interaction. The strength of the induced molecular coupling $G_{I\bar{I}}$ to the single coupling G_I is

$$G_{I\bar{I}} = \frac{G_I^2}{128\pi^4\rho^2}\xi \tag{6}$$

where the dimensionless and positive hopping parameter is defined as

$$\xi = \frac{1}{\rho^4}\int dud^4R[\rho T_{I\bar{I}}(u,R)]^{2N_f-2}. \tag{7}$$

In summary, we will use the effective action

$$\mathcal{L} = \bar{\psi}(i\partial\!\!\!/ - m)\psi + \mathcal{L}_I + \mathcal{L}_{I\bar{I}} \tag{8}$$

to describe light quark interactions in the QCD vacuum at low resolution. The smallness of the density $n_{I+\bar{I}}$ allows us to consider the complex many-body dynamics, by organizing it around the dilute limit. Throughout, we will use the $1/N_c$ counting for bookkeeping, with $n_{I+\bar{I}} \sim N_c$ and both G_I and $G_{I,\bar{I}}$ of the same order in $1/N_c$, but with a parametrically small ratio $G_{I\bar{I}}/G_I$ from the diluteness. With this in mind, the leading contributions in $1/N_c$ in (8) are

$$\mathcal{L}_I = \frac{G_I}{8N_c^2}[(\bar{\psi}\psi)^2-(\bar{\psi}\tau^a\psi)^2-(\bar{\psi}i\gamma^5\psi)^2+(\bar{\psi}i\gamma^5\tau^a\psi)^2],$$
$$\mathcal{L}_{I\bar{I}} = \frac{G_{I\bar{I}}}{2N_c^2}\Big[4[(\bar{\psi}\psi)^2+(\bar{\psi}\tau^a\psi)^2+(\bar{\psi}i\gamma^5\psi)^2+(\bar{\psi}i\gamma^5\tau^a\psi)^2]$$
$$-[(\bar{\psi}\gamma^\mu\psi)^2+(\bar{\psi}\tau^a\gamma^\mu\psi)^2-3(\bar{\psi}\gamma^\mu\gamma^5\psi)^2+(\bar{\psi}\tau^a\gamma^\mu\gamma^5\psi)^2]\Big]. \tag{9}$$

The induced 't Hooft interaction $\mathcal{L}_I$ does not operate in the light vector channels, but the molecular induced interaction $\mathcal{L}_{I\bar{I}}$ does. The molecular interaction is equally attractive in the scalar σ, a_0 and pseudoscalar π, η' channels. Since the instanton molecules are topologically neutral, the molecular interactions are $U(1)_A$ symmetric. Note that this Lagrangian predicts no splitting between the isoscalar (ω) and isovector (ρ) vector channels.

For later use, we rewrite (8) in leading order in $1/N_c$ as

$$\mathcal{L} = \bar{\psi}(i\partial\!\!\!/ - M)\psi + \frac{G_\sigma}{2}(\bar{\psi}\psi)^2 + \frac{G_{a_0}}{2}(\bar{\psi}\tau^a\psi)^2 + \frac{G_{\eta'}}{2}(\bar{\psi}i\gamma^5\psi)^2 + \frac{G_\pi}{2}(\bar{\psi}i\gamma^5\tau^a\psi)^2$$
$$-\frac{G_\omega}{2}(\bar{\psi}\gamma_\mu\psi)^2 - \frac{G_\rho}{2}(\bar{\psi}\gamma_\mu\tau^a\psi)^2 - \frac{G_{f_1}}{2}(\bar{\psi}\gamma_\mu\gamma^5\psi)^2 - \frac{G_{a_1}}{2}(\bar{\psi}\gamma_\mu\gamma^5\tau^a\psi)^2 \tag{10}$$

with the effective couplings

$$G_\sigma = G_S, \qquad G_{a_0} = -G_S + 8G_V,$$
$$G_\pi = G_S, \qquad G_{\eta'} = -G_S + 8G_V,$$
$$G_\omega = G_V, \qquad G_\rho = G_V,$$
$$G_{a_1} = G_V, \qquad G_{f_1} = -3G_V,$$

where $G_S = \frac{G_I}{4N_c^2} + \frac{4G_{I\bar{I}}}{N_c^2}$ and $G_V = \frac{G_{I\bar{I}}}{N_c^2}$ are from the QCD instanton vacuum.

B. Nonlocal approximation

Each instanton and anti-instanton configuration carries a finite size, which is fixed on average to be around $\frac{1}{3}$ fm. This size is not small in comparison to the size of the light hadrons and cannot be ignored. More importantly, this size fixes the UV scale and provides for a natural cutoff both in Euclidean and light front signature. Finite-sized instantons yield finite-sized zero modes, and therefore nonlocal effective interactions between the light quarks. The net effect is captured by the substitution

$$\psi(x) \to \sqrt{\mathcal{F}(i\partial)}\psi(x) \tag{11}$$

in the local approximation. Here $\mathcal{F}(i\partial)$ is the zero mode profile, that acts as a form factor. In singular gauge its form is more user friendly in momentum space

$$\mathcal{F}(k) = [(zF'(z))^2]\Big|_{z=\frac{k\rho}{2}} \tag{12}$$

where $F(z) = I_0(z)K_0(z) - I_1(z)K_1(z)$ are spherical Bessel functions, and $k = \sqrt{k^2}$ is the Euclidean 4-momentum.

Inserting (11) into (8) yields the nonlocal form of the effective action in the QCD instanton vacuum in leading order in $1/N_c$

$$\begin{aligned}\mathcal{L} = \bar\psi[i\not\partial - M(k)]\psi &+ \frac{G_S}{2}(\bar\psi\sqrt{\mathcal{F}(i\partial)}\sqrt{\mathcal{F}(i\partial)}\psi)^2 - \frac{G_S}{2}(\bar\psi\sqrt{\mathcal{F}(i\partial)}\tau^a\sqrt{\mathcal{F}(i\partial)}\psi)^2 \\ &- \frac{G_S}{2}(\bar\psi\sqrt{\mathcal{F}(i\partial)}i\gamma^5\sqrt{\mathcal{F}(i\partial)}\psi)^2 + \frac{G_S}{2}(\bar\psi\sqrt{\mathcal{F}(i\partial)}i\gamma^5\tau^a\sqrt{\mathcal{F}(i\partial)}\psi)^2 - \frac{G_V}{2}(\bar\psi\sqrt{\mathcal{F}(i\partial)}\gamma_\mu\sqrt{\mathcal{F}(i\partial)}\psi)^2 \\ &- \frac{G_V}{2}(\bar\psi\sqrt{\mathcal{F}(i\partial)}\gamma_\mu\tau^a\sqrt{\mathcal{F}(i\partial)}\psi)^2 + \frac{3G_V}{2}(\bar\psi\sqrt{\mathcal{F}(i\partial)}\gamma_\mu\gamma^5\sqrt{\mathcal{F}(i\partial)}\psi)^2 - \frac{G_V}{2}(\bar\psi\sqrt{\mathcal{F}(i\partial)}\gamma_\mu\gamma^5\tau^a\sqrt{\mathcal{F}(i\partial)}\psi)^2.\end{aligned} \tag{13}$$

III. GAP EQUATION IN QCD INSTANTON VACUUM

Before analyzing (13) in the light front frame, we briefly discuss the bulk vacuum properties following from (13) in the center-of-mass frame. In leading order in $1/N_c$ or mean-field approximation, the light quarks develop a running constituent mass

$$M(k) = m + 2g_S\mathcal{F}(k)\int\frac{d^4q}{(2\pi)^4}\frac{4M(q)}{q^2+M^2(q)}\mathcal{F}(q) \tag{14}$$

where $g_S = N_c G_S$ is the coupling strength for the isosinglet scalar channel in a 't Hooft Lagrangian. In the same approximation, the chiral quark condensate is

$$\begin{aligned}\langle\bar\psi\psi\rangle &= -\int\frac{d^4k}{(2\pi)^4}\mathrm{Tr}S(k) \\ &= -2N_c\int\frac{d^4k}{(2\pi)^4}\frac{4M(k)}{k^2+M^2(k)}\mathcal{F}(k).\end{aligned} \tag{15}$$

In the low momentum limit ($k \ll 1/\rho$), $M(k) \sim M\mathcal{F}(k)$ with M the zero-momentum constituent mass, (14) and (15) simplify to

$$\frac{m}{M} = 1 - 8g_S\int\frac{d^4k}{(2\pi)^4}\frac{\mathcal{F}^2(k)}{k^2+M^2} \tag{16}$$

with $M = m - G_S\langle\bar\psi\psi\rangle$. We have approximated the running quark mass $M(k)$ in the loop integration in both (14) and (15) by its zero momentum limit. This is numerically justified by the cutoff form factor $\mathcal{F}(k)$ with a range of about the inverse instanton size $1/\rho$.

More explicitly,

$$\frac{m}{M} = 1 - \frac{4g_S}{\pi^2\rho^2}\int_0^\infty dz\frac{z^3}{z^2+\frac{\rho^2M^2}{4}}(zF'(z))^4 \tag{17}$$

with M fixed by the scalar 't Hooft coupling strength g_S for fixed ρ. In the chiral limit, the constituent mass is nonzero only when the scalar coupling is stronger than the critical coupling g_S^{cr}, which is set by

$$g_S^{\mathrm{cr}} = 2\pi^2\rho^2\left[8\int_0^\infty dzz(zF'(z))^4\right]^{-1} \approx 2.981\pi^2\rho^2. \tag{18}$$

The small size expansion reduces the solution of the gap equation back to the point interaction limit, with both the quadratic $1/\rho$ and logarithmic dependence in $1/\rho$,

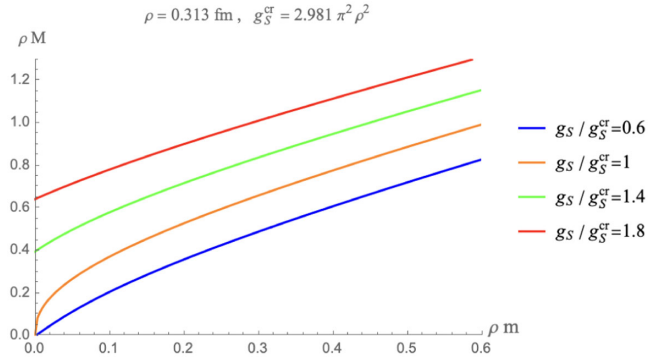

FIG. 1. Constituent mass as a function of the current mass with different scalar couplings g_S for a fixed instanton size $\rho = 0.31$ fm.

$$\frac{m}{M} = 1 - \frac{g_S}{2\pi^2\rho^2}\left[8\int_0^\infty dz z(zF'(z))^4 + \rho^2M^2\ln\rho^2M^2 + \mathcal{O}(\rho^2M^2)\right]. \tag{19}$$

This is to be compared to the cutoff scheme in the zero size limit, where the instanton size ρ in the QCD instanton vacuum provides a natural cutoff. Similarly, we have for the chiral quark condensate

$$\rho^3\langle\bar{\psi}\psi\rangle = -\frac{4N_c}{\pi^2}\rho M\int_0^\infty dz\frac{z^3}{z^2+\frac{\rho^2M^2}{4}}z(zF'(z))^2. \tag{20}$$

In the standard 2-flavor QCD instanton vacuum with $\rho \approx (636\ \text{MeV})^{-1}$, g_S^{cr} is approximately 72.64 GeV^{-2}. In Fig. 1 we show the constituent mass versus the current quark mass in units of the instanton size, for different scalar couplings g_S/g_S^{cr}. In Fig. 2 the constituent mass is shown versus g_S/g_S^{cr} for different current quark masses, with a clear onset of the spontaneously broken chiral phase. In Fig. 3 we show the chiral condensate versus g_S/g_S^{cr} for different current quark masses.

The effect of the instanton molecular contributions with $G_{I\bar{I}} \neq 0$ but parametrically small in comparison to G_I is seen to enhance the onset of the spontaneous breaking of

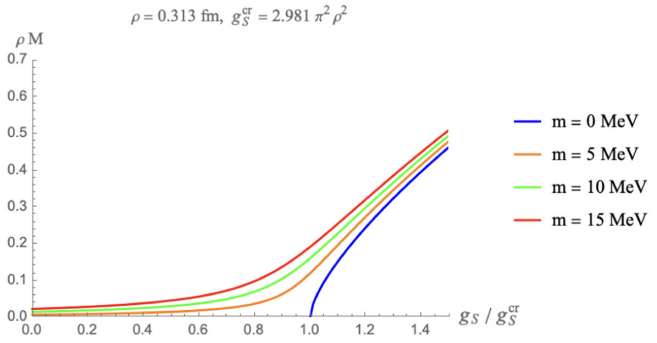

FIG. 2. Constituent quark mass versus the scalar coupling g_S.

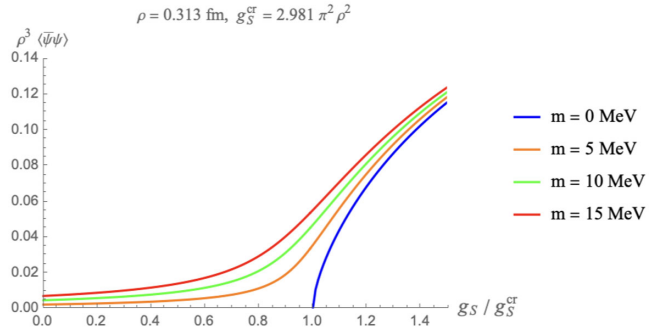

FIG. 3. Quark condensate as a function of the scalar coupling g_S.

chiral symmetry. This is readily seen by noting that (18) is now changed to

$$\frac{G_I}{4N_c}\left(1+\frac{G_I}{8\pi^2\rho^2N_c}\xi\right) \geq g_S^{cr} \approx 2.981\pi^2\rho^2 \tag{21}$$

with the positive hopping parameter ξ given in (7). In Fig. 4 we show the constituent quark mass versus the instanton density, for increasing values of the hopping parameter, in the chiral limit. The larger ξ, the smaller the instanton density required for the onset of chiral symmetry breaking. This effect is also illustrated in Fig. 5, where we show that a

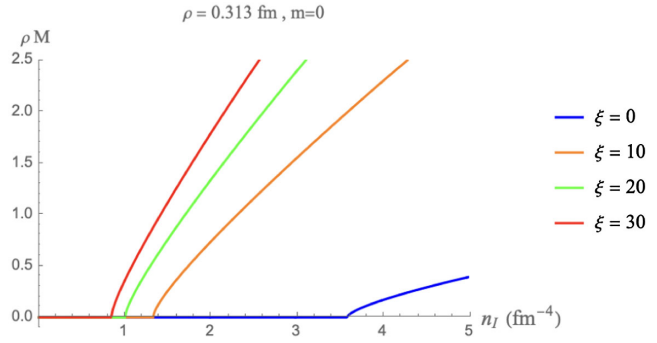

FIG. 4. Quark constituent mass in chiral limit as a function of instanton density in the presence of different ξ.

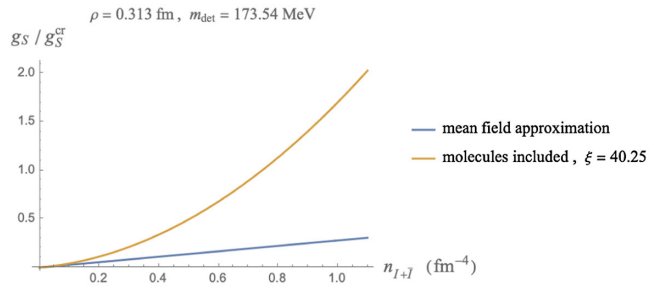

FIG. 5. The effective coupling g_S in σ channel as a function of instanton density.

lower instanton density is needed for a fixed scalar coupling in the presence of the molecular component.

IV. LIGHT FRONT FORMALISM OF NONLOCAL 't HOOFT LAGRANGIAN

On the light front, the spontaneous breaking of chiral symmetry in QCD follows from the emergent 't Hooft induced interactions, when the constrained part of the fermion field is eliminated [38]. This observation was initially made in the context of the NJL model in [56–58]. The projected fermion field along the light front yields a good plus bad component, with the latter nonpropagating or constrained. The elimination of the nonpropagating degrees of freedom induces the resummation of the multifermion interactions in terms of the good component. These interactions account for the spontaneous breaking of chiral symmetry on the light front through tadpoles.

More specifically, the fermionic constraint can be organized in $1/N_c$

$$\psi \to \psi_+ + \frac{\gamma^+}{2}\frac{-i}{\partial_-}(i\gamma^i_\perp\partial_i - M)\psi_+ + \mathcal{O}(G_S, G_V) \tag{22}$$

to render it manageable. The pair of fermion bilinears are of order $\mathcal{O}(\sqrt{N_c})$, compensating the $\mathcal{O}(1/N_c)$ contribution from the 't Hooft coupling $G_S = g_S/N_c$ and $G_V = g_V/N_c$. In leading order, the interactions on the light front are of order N_c^0. The light front effective theory follows from the integration of the bad component to the same order,

$$\mathcal{L} \to \bar\psi(i\partial\!\!\!/ - M)\psi - V(x) \tag{23}$$

with the local kernels (zero size instantons) after integration

$$V(x) = V^\sigma(x) + V^{a_0}(x) + V^\pi(x) + V^{\eta'}(x) + V^\omega(x) + V^\rho(x) + V^{a_1}(x) + V^{f_1}(x); \tag{24}$$

isoscalar σ channel:

$$V^\sigma(x) = -\frac{G_\sigma}{2}\bar\psi\psi\frac{1}{1 + G_\sigma\langle\bar\psi\gamma^+\frac{-i}{\partial_-}\psi\rangle}\bar\psi\psi; \tag{25}$$

isovector scalar channel:

$$V^{a_0}(x) = -\frac{G_{a_0}}{2}\bar\psi\tau^a\psi\frac{1}{1 + G_{a_0}\langle\bar\psi\gamma^+\frac{-i}{\partial_-}\psi\rangle}\bar\psi\tau^a\psi; \tag{26}$$

pion channel:

$$V^\pi(x) = -\frac{G_\pi}{2}\left(\bar\psi i\gamma^5\tau^a\psi + iG_{a_1}\left\langle\bar\psi\frac{-i}{\partial_-}\psi\right\rangle\bar\psi\gamma^+\gamma^5\tau^a\psi\right)\frac{1}{1 + G_\pi\langle\bar\psi\gamma^+\frac{-i}{\partial_-}\psi\rangle}\left(\bar\psi i\gamma^5\tau^a\psi + iG_{a_1}\left\langle\bar\psi\frac{-i}{\partial_-}\psi\right\rangle\bar\psi\gamma^+\gamma^5\tau^a\psi\right); \tag{27}$$

η' meson channel:

$$V^{\eta'}(x) = -\frac{G_{\eta'}}{2}\left(\bar\psi i\gamma^5\psi + iG_{f_1}\left\langle\bar\psi\frac{-i}{\partial_-}\psi\right\rangle\bar\psi\gamma^+\gamma^5\psi\right)\frac{1}{1 + G_{\eta'}\langle\bar\psi\gamma^+\frac{-i}{\partial_-}\psi\rangle}\left(\bar\psi i\gamma^5\psi + iG_{f_1}\left\langle\bar\psi\frac{-i}{\partial_-}\psi\right\rangle\bar\psi\gamma^+\gamma^5\psi\right); \tag{28}$$

isoscalar vector channel:

$$V^\omega(x) = \frac{G_\omega}{2}\bar\psi\gamma^i_\perp\psi\frac{1}{1 + G_\omega\langle\bar\psi\gamma^+\frac{-i}{\partial_-}\psi\rangle}\bar\psi\gamma_{i\perp}\psi + G_\omega\bar\psi\gamma^+\psi\left[\bar\psi\gamma^-\psi + G_\omega\left\langle\bar\psi\gamma^-\frac{-i}{\partial_-}\psi\right\rangle\bar\psi\gamma^+\psi\right]; \tag{29}$$

ρ meson channel:

$$V^\rho(x) = \frac{G_\rho}{2}\bar\psi\gamma^i_\perp\tau^a\psi\frac{1}{1 + G_\rho\langle\bar\psi\gamma^+\frac{-i}{\partial_-}\psi\rangle}\bar\psi\gamma_{i\perp}\tau^a\psi + G_\rho\bar\psi\gamma^+\tau^a\psi\left[\bar\psi\gamma^-\tau^a\psi + G_\rho\left\langle\bar\psi\gamma^-\frac{-i}{\partial_-}\psi\right\rangle\bar\psi\gamma^+\tau^a\psi\right]; \tag{30}$$

isovector axial vector channel:

$$V^{a_1}(x)=\frac{G_{a_1}}{2}\bar{\psi}\gamma^i_\perp\gamma^5\tau^a\psi\frac{1}{1+G_{a_1}\langle\bar{\psi}\gamma^+\frac{-i}{\partial_-}\psi\rangle}\bar{\psi}\gamma_{i\perp}\gamma^5\tau^a\psi+G_{a_1}\bar{\psi}\gamma^+\gamma^5\tau^a\psi\left[\bar{\psi}\gamma^-\gamma^5\tau^a\psi+G_{a_1}\left\langle\bar{\psi}\gamma^-\frac{-i}{\partial_-}\psi\right\rangle\bar{\psi}\gamma^+\gamma^5\tau^a\psi\right];\quad(31)$$

isoscalar axial vector channel:

$$V^{f_1}(x)=\frac{G_{f_1}}{2}\bar{\psi}\gamma^i_\perp\gamma^5\psi\frac{1}{1+G_{f_1}\langle\bar{\psi}\gamma^+\frac{-i}{\partial_-}\psi\rangle}\bar{\psi}\gamma_{i\perp}\gamma^5\psi+G_{f_1}\bar{\psi}\gamma^+\gamma^5\psi\left[\bar{\psi}\gamma^-\gamma^5\psi+G_{f_1}\left\langle\bar{\psi}\gamma^-\frac{-i}{\partial_-}\psi\right\rangle\bar{\psi}\gamma^+\gamma^5\psi\right].\quad(32)$$

For finite-sized instantons, the tadpole contributions in the emerging nonlocal kernels follow from the substitutions

$$\left\langle\bar{\psi}\gamma^+\frac{-i}{\partial_-}\psi\right\rangle\to\left\langle\bar{\psi}\mathcal{F}(i\partial)\gamma^+\frac{-i}{\partial_-}\mathcal{F}(i\partial)\psi\right\rangle,\quad(33)$$

$$\left\langle\bar{\psi}\frac{-i}{\partial_-}\psi\right\rangle\to\left\langle\bar{\psi}\mathcal{F}(i\partial)\frac{-i}{\partial_-}\mathcal{F}(i\partial)\psi\right\rangle,\quad(34)$$

$$\left\langle\bar{\psi}\gamma^-\frac{-i}{\partial_-}\psi\right\rangle\to\left\langle\bar{\psi}\mathcal{F}(i\partial)\gamma^-\frac{-i}{\partial_-}\mathcal{F}(i\partial)\psi\right\rangle,\quad(35)$$

which amount to the loop integrations in momentum space

$$\frac{1}{2N_c}\left\langle\bar{\psi}\mathcal{F}(i\partial)\gamma^+\frac{-i}{\partial_-}[\mathcal{F}(i\partial)\psi]\right\rangle\to w_+(P^+)=\int\frac{dk^+d^2k_\perp}{(2\pi)^3}\frac{\epsilon(k^+)}{P^+-k^+}\mathcal{F}(k)\mathcal{F}(P-k),\quad(36)$$

$$\frac{1}{2N_c}\left\langle\bar{\psi}\mathcal{F}(i\partial)\frac{-i}{\partial_-}[\mathcal{F}(i\partial)\psi]\right\rangle\to w_0(P^+)=\int\frac{dk^+d^2k_\perp}{(2\pi)^3}\frac{M\epsilon(k^+)}{k^+(P^+-k^+)}\mathcal{F}(k)\mathcal{F}(P-k),\quad(37)$$

$$\frac{1}{2N_c}\left\langle\bar{\psi}\mathcal{F}(i\partial)\gamma^-\frac{-i}{\partial_-}[\mathcal{F}(i\partial)\psi]\right\rangle\to w_-(P^+)=\int\frac{dk^+d^2k_\perp}{(2\pi)^3}\frac{(k^2_\perp+M^2)\epsilon(k^+)}{2(k^+)^2(P^+-k^+)}\mathcal{F}(k)\mathcal{F}(P-k).\quad(38)$$

The fermionic tadpole functions $w_\pm(P^+)$ are even in P^+, while $w_0(P^+)$ are odd in P^+.

A. Light front Hamiltonian

The emergent light front Hamiltonian for the QCD instanton vacuum with molecular contributions follows from the effective action (30) in the form

$$\begin{aligned}P^-=&\int[d^3k]_+\int[d^3q]_+\frac{k^2_\perp+M^2}{2k^+}\bar{\psi}(k)\gamma^+\psi(q)(2\pi)^3\delta^3_+(k-q)\\&+\int[d^3k]_+\int[d^3q]_+\int[d^3p]_+\int[d^3l]_+(2\pi)^3\delta^3_+(p+k-q-l)\sqrt{\mathcal{F}(k)\mathcal{F}(q)\mathcal{F}(p)\mathcal{F}(l)}V(k,q,p,l)\end{aligned}\quad(39)$$

with the shorthand notations

$$\int[d^3k]_+=\int\frac{dk^+d^2k_\perp}{(2\pi)^32k^+}\epsilon(k^+),\qquad\delta^3_+(k)=\delta(k^+)\delta^2(k_\perp).\quad(40)$$

The interaction kernel in (39) is given by

$$V(k,q,p,l)=\sum_{s_1,s_1',s_2,s_2'}\mathcal{V}_{s_1,s_2,s_1',s_2'}(k,q,p,l)b^\dagger_{s_1}(k)c^\dagger_{s_2}(q)c_{s_2'}(p)b_{s_1'}(l)\quad(41)$$

with the transition amplitude $\mathcal{V}_{s_1,s_2,s_1',s_2'}(k,q,p,l)$ summing over the eight meson channels,

$$\mathcal{V}_{s_1,s_2,s_1',s_2'}(k,q,p,l)=\mathcal{V}^{\sigma}_{s_1,s_2,s_1',s_2'}(k,q,p,l)+\mathcal{V}^{\eta'}_{s_1,s_2,s_1',s_2'}(k,q,p,l)+\mathcal{V}^{\pi}_{s_1,s_2,s_1',s_2'}(k,q,p,l)+\mathcal{V}^{a_0}_{s_1,s_2,s_1',s_2'}(k,q,p,l)$$
$$+\mathcal{V}^{\omega}_{s_1,s_2,s_1',s_2'}(k,q,p,l)+\mathcal{V}^{\rho}_{s_1,s_2,s_1',s_2'}(k,q,p,l)+\mathcal{V}^{a_1}_{s_1,s_2,s_1',s_2'}(k,q,p,l)+\mathcal{V}^{f_1}_{s_1,s_2,s_1',s_2'}(k,q,p,l); \quad (42)$$

isoscalar scalar σ channel:

$$\mathcal{V}^{\sigma}_{s_1,s_2,s_1',s_2'}(k,q,p,l)=-\frac{g_\sigma}{N_c}\frac{1}{1+2g_\sigma w_+(P^+)}\bar{u}_{s_1}(k)v_{s_2}(q)\bar{v}_{s_2'}(l)u_{s_1'}(p); \quad (43)$$

isovector scalar a_0 channel:

$$\mathcal{V}^{a_0}_{s_1,s_2,s_1',s_2'}(k,q,p,l)=-\frac{g_{a_0}}{N_c}\frac{1}{1+2g_{a_0}w_+(P^+)}\bar{u}_{s_1}(k)\tau^a v_{s_2}(q)\bar{v}_{s_2'}(l)\tau^a u_{s_1'}(p); \quad (44)$$

pion channel:

$$\mathcal{V}^{\pi}_{s_1,s_2,s_1',s_2'}(k,q,p,l)=-\frac{g_\pi}{N_c}\frac{1}{1+2g_\pi w_+(P^+)}[\bar{u}_{s_1}(k)i\gamma^5\tau^a v_{s_2}(q)+2ig_{a_1}w_0(P^+)\bar{u}_{s_1}(k)\gamma^+\gamma^5\tau^a v_{s_2}(q)]$$
$$\times[\bar{v}_{s_2'}(l)i\gamma^5\tau^a u_{s_1'}(p)-2ig_{a_1}w_0(P^+)\bar{v}_{s_2'}(l)\gamma^+\gamma^5\tau^a u_{s_1'}(p)]; \quad (45)$$

η' meson channel:

$$\mathcal{V}^{\eta'}_{s_1,s_2,s_1',s_2'}(k,q,p,l)=-\frac{g_{\eta'}}{N_c}\frac{1}{1+2g_{\eta'}w_+(P^+)}[\bar{u}_{s_1}(k)i\gamma^5 v_{s_2}(q)+2ig_{f_1}w_0(P^+)\bar{u}_{s_1}(k)\gamma^+\gamma^5 v_{s_2}(q)]$$
$$\times[\bar{v}_{s_2'}(l)i\gamma^5 u_{s_1'}(p)-2ig_{f_1}w_0(P^+)\bar{v}_{s_2'}(l)\gamma^+\gamma^5 u_{s_1'}(p)]; \quad (46)$$

isoscalar vector channel:

$$\mathcal{V}^{\omega}_{s_1,s_2,s_1',s_2'}(k,q,p,l)=\frac{g_\omega}{N_c}\frac{1}{1+2g_\omega w_+(P^+)}\bar{u}_{s_1}(k)\gamma^i_\perp v_{s_2}(q)\bar{v}_{s_2'}(l)\gamma_{i\perp}u_{s_1'}(p)$$
$$+\frac{g_\omega}{N_c}\bar{u}_{s_1}(k)\gamma^+ v_{s_2}(q)[\bar{v}_{s_2'}(l)\gamma^- u_{s_1'}(p)+2g_\omega w_-(P^+)\bar{v}_{s_2'}(l)\gamma^+ u_{s_1'}(p)]$$
$$+\frac{g_\omega}{N_c}[\bar{u}_{s_1}(k)\gamma^- v_{s_2}(q)+2g_\omega w_-(P^+)\bar{u}_{s_1}(k)\gamma^+ v_{s_2}(q)]\bar{v}_{s_2'}(l)\gamma^+ u_{s_1'}(p); \quad (47)$$

ρ meson channel:

$$\mathcal{V}^{\rho}_{s_1,s_2,s_1',s_2'}(k,q,p,l)=\frac{g_\rho}{N_c}\frac{1}{1+2g_\rho w_+(P^+)}\bar{u}_{s_1}(k)\gamma^i_\perp\tau^a v_{s_2}(q)\bar{v}_{s_2'}(l)\gamma_{i\perp}\tau^a u_{s_1'}(p)$$
$$+\frac{g_\rho}{N_c}\bar{u}_{s_1}(k)\gamma^+\tau^a v_{s_2}(q)[\bar{v}_{s_2'}(l)\gamma^-\tau^a u_{s_1'}(p)+2g_\rho w_-(P^+)\bar{v}_{s_2'}(l)\gamma^+\tau^a u_{s_1'}(p)]$$
$$+\frac{g_\rho}{N_c}[\bar{u}_{s_1}(k)\gamma^-\tau^a v_{s_2}(q)+2g_\rho w_-(P^+)\bar{u}_{s_1}(k)\gamma^+\tau^a v_{s_2}(q)]\bar{v}_{s_2'}(l)\gamma^+\tau^a u_{s_1'}(p); \quad (48)$$

isotriplet axial vector channel:

$$\mathcal{V}^{a_1}_{s_1,s_2,s_1',s_2'}(k,q,p,l)=\frac{g_{a_1}}{N_c}\frac{1}{1+2g_{a_1}w_+(P^+)}\bar{u}_{s_1}(k)\gamma^i_\perp\gamma^5\tau^a v_{s_2}(q)\bar{v}_{s_2'}(l)\gamma_{i\perp}\gamma^5\tau^a u_{s_1'}(p)$$
$$+\frac{g_{a_1}}{N_c}\bar{u}_{s_1}(k)\gamma^+\gamma^5\tau^a v_{s_2}(q)[\bar{v}_{s_2'}(l)\gamma^-\gamma^5\tau^a u_{s_1'}(p)+2g_{a_1}w_-(P^+)\bar{v}_{s_2'}(l)\gamma^+\gamma^5\tau^a u_{s_1'}(p)]$$
$$+\frac{g_{a_1}}{N_c}[\bar{u}_{s_1}(k)\gamma^-\gamma^5\tau^a v_{s_2}(q)+2g_{a_1}w_-(P^+)\bar{u}_{s_1}(k)\gamma^+\gamma^5\tau^a v_{s_2}(q)]\bar{v}_{s_2'}(l)\gamma^+\gamma^5\tau^a u_{s_1'}(p); \quad (49)$$

isoscalar axial vector channel:

$$\mathcal{V}^{f_1}_{s_1,s_2,s_1',s_2'}(k,q,p,l) = \frac{g_{f_1}}{N_c}\frac{1}{1+2g_{f_1}w_+(P^+)}\bar{u}_{s_1}(k)\gamma^i_\perp\gamma^5 v_{s_2}(q)\bar{v}_{s_2'}(l)\gamma_{i\perp}\gamma^5 u_{s_1'}(p)$$
$$+\frac{g_{f_1}}{N_c}\bar{u}_{s_1}(k)\gamma^+\gamma^5 v_{s_2}(q)[\bar{v}_{s_2'}(l)\gamma^-\gamma^5 u_{s_1'}(p)+2g_{f_1}w_-(P^+)\bar{v}_{s_2'}(l)\gamma^+\gamma^5 u_{s_1'}(p)]$$
$$+\frac{g_{f_1}}{N_c}[\bar{u}_{s_1}(k)\gamma^-\gamma^5 v_{s_2}(q)+2g_{f_1}w_-(P^+)\bar{u}_{s_1}(k)\gamma^+\gamma^5 v_{s_2}(q)]\bar{v}_{s_2'}(l)\gamma^-\gamma^5 u_{s_1'}(p), \tag{50}$$

where $g_X = N_c G_X$.

B. Bound state equations

The light scalar and vector eigenstates to the light front Hamiltonian (39) can be formally sought in the following form

$$|\text{Meson } X,\lambda,P\rangle = \int_0^1 \frac{dx}{\sqrt{2x\bar{x}}}\int\frac{d^2k_\perp}{(2\pi)^3}\sum_{s_1,s_2}\Phi^\lambda_X(x,k_\perp,s_1,s_2)b^\dagger_{s_1}(k)c^\dagger_{s_2}(P-k)|0\rangle \tag{51}$$

with $\lambda=\pm$ (transverse) and $\lambda=0$ (longitudinal) polarizations of the X-vector mesons. The polarization label is absent for the X-scalar mesons. In the QCD instanton vacuum, the pertinent eigenequation for the X-meson on the light front is

$$m_X^2\Phi^\lambda_X(x,k_\perp,s_1,s_2) = \frac{k_\perp^2+M^2}{x\bar{x}}\Phi^\lambda_X(x,k_\perp,s_1,s_2)+\frac{1}{\sqrt{2x\bar{x}}}\sqrt{\mathcal{F}(k)\mathcal{F}(P-k)}$$
$$\times\int_0^1\frac{dy}{\sqrt{2y\bar{y}}}\int\frac{d^2q_\perp}{(2\pi)^3}\sum_{s,s'}\mathcal{V}_{s_1,s_2,s,s'}(k,P-k,q,P-q)\Phi^\lambda_X(y,q_\perp,s,s')\sqrt{\mathcal{F}(q)\mathcal{F}(P-q)} \tag{52}$$

using the $1/N_c$ bookkeeping.

Throughout, we will be mostly interested in the vector (spin-1) mesons, as the scalar (spin-0) mesons were already discussed in [38], to which we refer the reader to for further details. Here, the scalars are kept solely for the purpose of comparison to the vector results. Also, the diluteness of the instanton tunneling rate in the QCD vacuum yields a parametrically small G_V/G_S ratio, with minor changes in the vacuum parameters as we discussed earlier. Hence, only the leading contribution in G_V in the bound state problem will be kept. As a result, the (pseudo)scalar-axial-vector mixing of order G_V/G_S will be ignored. With this in mind, we now detail the interaction kernels for the scalar and vector channels and their corresponding bound state equations.

1. Scalar channels

$$\sum_{s,s'}\mathcal{V}^\sigma_{s,s',s_1,s_2}(q,q',k,k')\Phi_\sigma(y,q_\perp,s,s') = -\frac{4g_\sigma}{1+2g_\sigma w_+(P^+)}\left(\frac{q_\perp^2+(y-\bar{y})^2M^2}{y\bar{y}}\right)\phi_\sigma(y,q_\perp)\bar{u}_{s_1}(k)v_{s_2}(k'), \tag{53}$$

$$\sum_{s,s'}\mathcal{V}^{a_0}_{s,s',s_1,s_2}(q,q',k,k')\Phi_{a_0}(y,q_\perp,s,s') = -\frac{4g_{a_0}}{1+2g_{a_0}w_+(P^+)}\left(\frac{q_\perp^2+(y-\bar{y})^2M^2}{y\bar{y}}\right)\phi_{a_0}(y,q_\perp)\bar{u}_{s_1}(k)\tau^a v_{s_2}(k'), \tag{54}$$

where $g_\sigma = g_S$ and $g_{a_0} = -g_S + 8g_V$.

2. Pseudoscalar channels

$$\sum_{s,s'}\mathcal{V}^\pi_{s,s',s_1,s_2}(q,q',k,k')\Phi_\pi(y,q_\perp,s,s') = -\frac{4g_\pi}{1+2g_\pi w_+(P^+)}\left(\frac{q_\perp^2+M^2}{y\bar{y}}\right)\phi_\pi(y,q_\perp)\bar{u}_{s_1}(k)i\gamma^5\tau^a v_{s_2}(k'), \tag{55}$$

$$\sum_{s,s'}\mathcal{V}^{\eta'}_{s,s',s_1,s_2}(q,q',k,k')\Phi_{\eta'}(y,q_\perp,s,s')=-\frac{4g_{\eta'}}{1+2g_{\eta'}w_+(P^+)}\left(\frac{q_\perp^2+M^2}{y\bar{y}}\right)\phi_{\eta'}(y,q_\perp)\bar{u}_{s_1}(k)i\gamma^5 v_{s_2}(k'), \tag{56}$$

with $g_\sigma=g_S$ and $g_{a_0}=-g_S+8g_V$.

3. Vector channels

Transverse polarization states:

$$\sum_{s,s'}\mathcal{V}^{\omega}_{s_1,s_2,s,s'}(k,k',q,q')\Phi^{\pm}_{\omega}(y,q_\perp,s,s')=-\frac{4g_\omega}{1+2g_\omega w_+(P^+)}\left(\frac{q_\perp^2+M^2-2y\bar{y}q_\perp^2}{y\bar{y}}\right)\phi_\omega(y,q_\perp)\epsilon_i^{\pm}(P)\bar{u}_{s_1}(k)\gamma^i_\perp v_{s_2}(k'); \tag{57}$$

$$\sum_{s,s'}\mathcal{V}^{\rho}_{s_1,s_2,s,s'}(k,k',q,q')\Phi^{\pm}_{\rho}(y,q_\perp,s,s')=-\frac{4g_\rho}{1+2g_\rho w_+(P^+)}\left(\frac{q_\perp^2+M^2-2y\bar{y}q_\perp^2}{y\bar{y}}\right)\phi_\rho(y,q_\perp)\epsilon_i^{\pm}(P)\bar{u}_{s_1}(k)\tau^a\gamma^i_\perp v_{s_2}(k'); \tag{58}$$

longitudinal polarization states:

$$\begin{aligned}
&\sum_{s,s'}\mathcal{V}^{\omega}_{s_1,s_2,s,s'}(k,k',q,q')\Phi^{0}_{\omega}(y,q_\perp,s,s')\\
&=-8g_\omega\left[\frac{q_\perp^2+M^2}{y\bar{y}}-4g_\omega w_-(P^+)(P^+)^2\right]y\bar{y}\left(1+\frac{q_\perp^2+M^2}{m_\omega^2 y\bar{y}}\right)\phi_\omega(y,q_\perp)\left[-\frac{m_\omega}{2P^+}\bar{u}_{s_1}(k)\gamma^+ v_{s_2}(P-k)\right]\\
&\quad-8g_\omega\left[\frac{k_\perp^2+M^2}{x\bar{x}}-4g_\omega w_-(P^+)(P^+)^2\right]y\bar{y}\left(1+\frac{q_\perp^2+M^2}{m_\omega^2 y\bar{y}}\right)\phi_\omega(y,q_\perp)\left[-\frac{m_\omega}{2P^+}\bar{u}_{s_1}(k)\gamma^+ v_{s_2}(P-k)\right],
\end{aligned} \tag{59}$$

$$\begin{aligned}
&\sum_{s,s'}\mathcal{V}^{\rho}_{s_1,s_2,s,s'}(k,k',q,q')\Phi^{0}_{\rho}(y,q_\perp,s,s')\\
&=-8g_\rho\left[\frac{q_\perp^2+M^2}{y\bar{y}}-4g_\rho w_-(P^+)(P^+)^2\right]y\bar{y}\left(1+\frac{q_\perp^2+M^2}{m_\rho^2 y\bar{y}}\right)\phi_\rho(y,q_\perp)\left[-\frac{m_\rho}{2P^+}\bar{u}_{s_1}(k)\gamma^+\tau^a v_{s_2}(P-k)\right]\\
&\quad-8g_\rho\left[\frac{k_\perp^2+M^2}{x\bar{x}}-4g_\rho w_-(P^+)(P^+)^2\right]y\bar{y}\left(1+\frac{q_\perp^2+M^2}{m_\rho^2 y\bar{y}}\right)\phi_\rho(y,q_\perp)\left[-\frac{m_\rho}{2P^+}\bar{u}_{s_1}(k)\gamma^+\tau^a v_{s_2}(P-k)\right],
\end{aligned} \tag{60}$$

with $g_\omega=g_\rho=g_V$. The minus component of the spinor wave function can be traded for the plus component

$$\epsilon_0^\mu(P)\bar{u}_{s_1}(k)\gamma_\mu v_{s_2}(P-k)=-\frac{m_X}{2P^+}\left(1+\frac{k_\perp^2+M^2}{m_X^2 x\bar{x}}\right)\bar{u}_{s_1}(k)\gamma^+ v_{s_2}(P-k) \tag{61}$$

thanks to the longitudinal Ward identity

$$\bar{u}_{s_1}(k)\gamma^- v_{s_2}(P-k)=-\frac{1}{(P^+)^2}\frac{k_\perp^2+M^2}{2x\bar{x}}\bar{u}_{s_1}(k)\gamma^+ v_{s_2}(P-k). \tag{62}$$

On the light front, the longitudinal and transverse polarizations appear decoupled, yet underlying this is hidden Lorentz symmetry. This will be recovered below in details both in the spectrum and ensuing longitudinal wave functions.

4. Bound state equations for each channel

Scalar channels:

$$m^2_{\sigma,a_0}\phi_{\sigma,a_0}(x,k_\perp) = \frac{k_\perp^2+M^2}{x\bar{x}}\phi_{\sigma,a_0}(x,k_\perp) - \frac{4g_{\sigma,a_0}}{\sqrt{2x\bar{x}}}\frac{\sqrt{\mathcal{F}(k)\mathcal{F}(P-k)}}{1+2g_{\sigma,a_0}w_+(P^+)} \times \int\frac{dy}{\sqrt{2y\bar{y}}}\int\frac{d^2q_\perp}{(2\pi)^3}\left(\frac{q_\perp^2+(y-\bar{y})^2M^2}{y\bar{y}}\right)\phi_{\sigma,a_0}(y,q_\perp)\sqrt{\mathcal{F}(q)\mathcal{F}(P-q)}; \tag{63}$$

pseudoscalar channels:

$$m^2_{\pi,\eta'}\phi_{\pi,\eta'}(x,k_\perp) = \frac{k_\perp^2+M^2}{x\bar{x}}\phi_{\pi,\eta'}(x,k_\perp) - \frac{4g_{\pi,\eta'}}{\sqrt{2x\bar{x}}}\frac{\sqrt{\mathcal{F}(k)\mathcal{F}(P-k)}}{1+2g_{\pi,\eta'}w_+(P^+)} \times \int\frac{dy}{\sqrt{2y\bar{y}}}\int\frac{d^2q_\perp}{(2\pi)^3}\left(\frac{q_\perp^2+M^2}{y\bar{y}}\right)\phi_{\pi,\eta'}(y,q_\perp)\sqrt{\mathcal{F}(q)\mathcal{F}(P-q)}; \tag{64}$$

transverse vector channels:

$$m^2_{\omega,\rho}\phi_{\omega,\rho}(x,k_\perp) = \frac{k_\perp^2+M^2}{x\bar{x}}\phi_{\omega,\rho}(x,k_\perp) - \frac{4g_{\omega,\rho}}{\sqrt{2x\bar{x}}}\frac{\sqrt{\mathcal{F}(k)\mathcal{F}(P-k)}}{1+2g_{\omega,\rho}w_+(P^+)} \times \int\frac{dy}{\sqrt{2y\bar{y}}}\int\frac{d^2q_\perp}{(2\pi)^3}\left(\frac{q_\perp^2+M^2-2y\bar{y}q_\perp^2}{y\bar{y}}\right)\phi_{\omega,\rho}(y,q_\perp)\sqrt{\mathcal{F}(q)\mathcal{F}(P-q)}; \tag{65}$$

longitudinal vector channels:

$$m^2_{\omega,\rho}\phi_{\omega,\rho}(x,k_\perp) = \frac{k_\perp^2+M^2}{x\bar{x}}\phi_{\omega,\rho}(x,k_\perp) - \frac{4g_{\omega,\rho}}{\sqrt{2x\bar{x}}}\sqrt{\mathcal{F}(k)\mathcal{F}(P-k)} \times \int\frac{dy}{\sqrt{2y\bar{y}}}\int\frac{d^2q_\perp}{(2\pi)^3}4(q_\perp^2+M^2)\phi_{\omega,\rho}(y,q_\perp)\sqrt{\mathcal{F}(q)\mathcal{F}(P-q)}. \tag{66}$$

The derivation of the bound state equation for the longitudinal channel is more challenging, with the details given in Appendix B. The asymmetry between the longitudinal and transverse channels reflects on the lack of manifest Lorentz symmetry on the light front. However, a closer analysis shows that the longitudinal and transverse mass eigenstates are equal, and that the longitudinal and transverse distribution amplitudes are tied by covariance.

C. Meson spectrum

The eigenvalues to the bound state equations for each of the meson channels determine the mass spectrum in the light front formalism. In fact, the eigenvalue problem can be recast into an integral equation for the mass spectrum. For this, we note that the tadpole function $w_+(P^+)$ controlling the emergent vertices can be recast as follows

$$\begin{aligned} w_+(P^+) &= \int\frac{dk^+d^2k_\perp}{(2\pi)^3}\frac{\epsilon(k^+)}{P^+-k^+}\mathcal{F}(k)\mathcal{F}(P-k) \\ &= \int_0^1 dx\int\frac{d^2k_\perp}{(2\pi)^3}\frac{2}{x}\mathcal{F}(k)\mathcal{F}(P-k) - \int\frac{dk^+d^2k_\perp}{(2\pi)^3}\frac{\epsilon(k^+)}{k^+}\mathcal{F}(P-k)\mathcal{F}(k) \\ &\simeq \int_0^1 dx\int\frac{d^2k_\perp}{(2\pi)^3}\frac{2}{x}\mathcal{F}(k)\mathcal{F}(P-k) - \frac{1}{2g_S}\left(1-\frac{m}{M}\right) \end{aligned} \tag{67}$$

where we used

$$\int\frac{dk^+d^2k_\perp}{(2\pi)^3}\frac{\epsilon(k^+)}{k^+}[\mathcal{F}(k)\mathcal{F}(P-k)] \simeq \frac{1}{2g_S}\left(1-\frac{m}{M}\right). \tag{68}$$

With this in mind, the eigenvalue equations (63)–(66) can be recast in the form of gaplike equations, much like the vacuum parameters discussed earlier. More specifically, we obtain the following:

scalar modes:

$$1-\frac{g_{\sigma,a_0}}{g_S}\left(1-\frac{m}{M}\right)=-2g_{\sigma,a_0}(m^2_{\sigma,a_0}-4M^2)\int_0^1 dx\int\frac{d^2k_\perp}{(2\pi)^3}\frac{1}{x\bar{x}m^2_{\sigma,a_0}-(k^2_\perp+M^2)}\mathcal{F}(k)\mathcal{F}(P-k); \tag{69}$$

pseudoscalar modes:

$$1-\frac{g_{\pi,\eta'}}{g_S}\left(1-\frac{m}{M}\right)=-2g_{\pi,\eta'}m^2_{\pi,\eta'}\int_0^1 dx\int\frac{d^2k_\perp}{(2\pi)^3}\frac{1}{x\bar{x}m^2_{\pi,\eta'}-(k^2_\perp+M^2)}\mathcal{F}(k)\mathcal{F}(P-k); \tag{70}$$

transverse modes:

$$1-\frac{g_{\omega,\rho}}{g_S}\left(1-\frac{m}{M}\right)=-2g_{\omega,\rho}\int_0^1 dx\int\frac{d^2k_\perp}{(2\pi)^3}\frac{m^2_{\omega,\rho}-2k^2_\perp}{x\bar{x}m^2_{\omega,\rho}-(k^2_\perp+M^2)}\mathcal{F}(k)\mathcal{F}(P-k); \tag{71}$$

longitudinal modes:

$$1=-8g_{\omega,\rho}\int_0^1 dx\int\frac{d^2k_\perp}{(2\pi)^3}\frac{k^2_\perp+M^2}{x\bar{x}m^2_{\omega,\rho}-(k^2_\perp+M^2)}\mathcal{F}(k)\mathcal{F}(P-k). \tag{72}$$

Despite the apparent difference between the longitudinal and transverse kernels, the mass solutions are the same.

D. Meson spectrum in covariant formalism

For comparison, we now briefly derive the mass spectra for the light mesons in the covariant frame, by using the standard Bethe-Salpeter construction for bound states. Using the $1/N_c$ bookkeeping, we can resum the leading contributions to the 4-point function diagrammatically as follows:

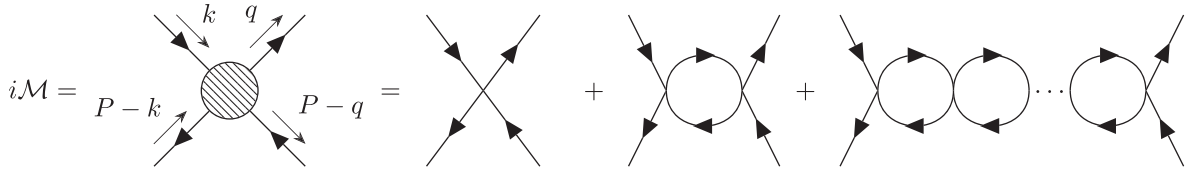

The diagrammatic rules follow from the effective action detailed in Appendix A. Since we are chiefly interested in the mass eigenvalue equation for scalar and vector mesons in this covariant formulation, it is sufficient to note that the on-shell condition $P^2=m^2_X$ of the intermediate meson state $X=\sigma,a_0,\omega,\rho,\eta',\pi$ is respectively,

$$\begin{aligned}1&=G_{\sigma,a_0}\Pi_{SS}(m^2_{\sigma,a_0}),\\ 1&=G_{\omega,\rho}\Pi_{VV}(m^2_{\omega,\rho}),\\ 1&=G_{\eta',\pi}\Pi_{PP}(m^2_{\eta',\pi}),\end{aligned} \tag{73}$$

where each vacuum polarization function is defined as

$$\begin{aligned}\Pi_{SS}&=4N_c(P^2-4M^2)I_1(P^2)+8N_cI_2(P^2),\\ \Pi_{PP}&=4N_cP^2I_1(P^2)+8N_cI_2(P^2),\\ \Pi_{VV}&=\frac{8}{3}N_c(P^2+2M^2)I_1(P^2)+\frac{16}{3}N_cI_2(P^2),\end{aligned} \tag{74}$$

with the one-loop integrals

$$I_1(P^2) = \int \frac{d^4k}{(2\pi)^4} \frac{-i}{[(k-P/2)^2 - M^2][(k+P/2)^2 - M^2]} \mathcal{F}(k-P/2)\mathcal{F}(k+P/2),$$
$$I_2(P^2) = \int \frac{d^4k}{(2\pi)^4} \frac{i}{k^2 - M^2} \mathcal{F}(k)\mathcal{F}(P-k). \tag{75}$$

Equation (73) defines implicitly the mass spectra in a covariant frame. We note that in the pseudoscalar channel, the resumation of the vacuum polarization in the pion channel can receive additional contributions from $\pi - a_1$ and $\eta' - f_1$ mixing. However, these mixing contributions are suppressed in $1/N_c$ or G_V/G_S, much like in the light front case. The interactions in the σ, a_0, π, η', ω, and ρ channels are attractive, and we expect binding for a given range of couplings. The on-shell conditions (73) can be rearranged by noting that

$$I_2(P^2) \simeq \int \frac{d^4k}{(2\pi)^4} \frac{i}{k^2 - M^2} \mathcal{F}^2(k) = \frac{1}{8g_S}\left(1 - \frac{m}{M}\right). \tag{76}$$

Inserting (76) into (75) and then in (73) yields the gaplike equations for the mass spectra in a covariant frame:

$$1 - \frac{g_{\sigma,a_0}}{g_\sigma}\left(1 - \frac{m}{M}\right) = -4g_{\sigma,a_0}(m^2_{\sigma,a_0} - 4M^2) \int \frac{d^4k}{(2\pi)^4} \frac{i}{(k^2 - M^2)[(P-k)^2 - M^2]} \mathcal{F}(k)\mathcal{F}(P-k),$$
$$1 - \frac{g_{\pi,\eta'}}{g_\sigma}\left(1 - \frac{m}{M}\right) = -4g_{\pi,\eta'} m^2_{\pi,\eta'} \int \frac{d^4k}{(2\pi)^4} \frac{i}{(k^2 - M^2)[(P-k)^2 - M^2]} \mathcal{F}(k)\mathcal{F}(P-k),$$
$$1 - \frac{2g_{\omega,\rho}}{3g_\sigma}\left(1 - \frac{m}{M}\right) = -\frac{8}{3} g_{\omega,\rho}(m^2_{\omega,\rho} + 2M^2) \int \frac{d^4k}{(2\pi)^4} \frac{i}{(k^2 - M^2)[(P-k)^2 - M^2]} \mathcal{F}(k)\mathcal{F}(P-k). \tag{77}$$

E. Connection to the light front

While in the light front formulation manifest Lorentz symmetry is irremediably lost, the mass spectra should be identical. To show this equivalence in our case, it is best to carry the integrations in (77) by splitting the measure $d^4k \to dk^- dk^+ dk_\perp$, and carrying first the k^- integration in $I_1(P^2)$,

$$\int_{-\infty}^{\infty} \frac{dk^-}{2\pi} \frac{i}{(k^2 - M^2)[(P-k)^2 - M^2]} \mathcal{F}(k)\mathcal{F}(P-k)\Big|_{P^2 = m_X^2}$$
$$\to \frac{\theta(x\bar{x})}{2x\bar{x}P^+} \frac{1}{m_X^2 - \frac{k_\perp^2 + M^2}{x\bar{x}}} [zF'(z)]^4\Big|_{z = \frac{\rho k_\perp}{2\lambda_X \sqrt{x\bar{x}}}}. \tag{78}$$

This can be justified by doing the contour integral along $k'^4 = \frac{-k^3 + ik^4}{\sqrt{2}}$ in Euclidean space. The parameter λ_X is of order 1 and can be determined by matching the integrals on both sides. They arise from the process of removing the spurious poles in the two-body nonlocal form factor in the analytical continuation from Euclidean to Minkowski signature [59,60]. Effectively, the parameter λ_X is a measure of the nonlocality related to the finite-sized instanton vacuum with effective size cutoff ρ/λ_X which depends on the bound state mass m_X, constituent mass M, and instanton size ρ. We will use λ_S for the vertices emerging from single instantons, and λ_V for the vertices emerging from the molecules. Following [59,60], we fix them empirically by the weak decay constants (see below),

$$\lambda_S = 2.464, \qquad \lambda_V = 3.542. \tag{79}$$

Inserting (78) into (77) yields the same gaplike equations obtained in the light front, as expected. We now proceed to solve numerically these gaplike equations to display the scalar and vector spectra.

1. Scalar sigma channel

$$\frac{m}{M} = \frac{g_S}{2\pi^2}(m_\sigma^2 - 4M^2) \int_0^1 dx \times \int_0^\infty dz \frac{z}{z^2 - \frac{\rho^2}{4\lambda_S}\left(m_\sigma^2 - \frac{M^2}{x\bar{x}}\right)} [zF'(z)]^4. \tag{80}$$

In Fig. 6 we show the sigma mass m_σ (solid line) versus the current mass m for a fixed instanton size $\rho = 0.31$ fm and scalar coupling, all in units of ρ. The dashed line is the $2M$ threshold. The σ meson is a threshold state in the chiral limit and becomes unbound away from the chiral limit. For $g_S = 2.54 \times 2\pi^2\rho^2$, the σ mass is $m_\sigma = 2M = 743.1$ MeV in the chiral limit.

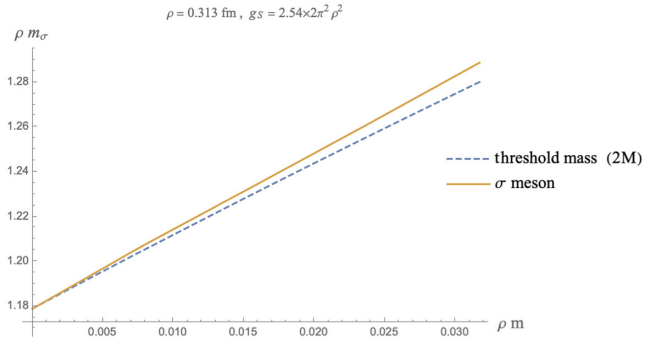

FIG. 6. Sigma mass versus the current quark mass. solid line. The dashed line is the 2M threshold.

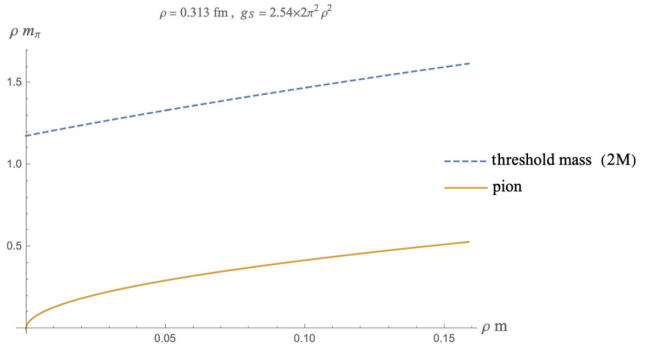

FIG. 7. Pion mass versus the current quark mass, solid line. The dashed line is the 2M threshold.

2. Pseudoscalar pion channel

$$\frac{m}{M}=\frac{g_S}{2\pi^2}m_\pi^2\int_0^1 dx\int_0^\infty dz\frac{z}{z^2-\frac{\rho^2}{4\lambda_S^2}\left(m_\pi^2-\frac{M^2}{x\bar{x}}\right)}[zF'(z)]^4. \tag{81}$$

In Fig. 7 we show the pion mass m_σ (solid line) versus the current mass m for a fixed instanton size $\rho = 0.31$ fm and scalar coupling, all in units of ρ. The dashed line is the $2M$ threshold. In comparison to the scalar channel, the pion channel is strongly attractive in the QCD instanton vacuum. Flavor $SU(2)$ symmetry guarantees $g_\sigma = g_\pi = g_S$. In particular, the chiral expansion of the pion mass eigenvalue or gaplike equation yields the Gell-Mann-Oakes-Renner relation

$$m_\pi^2=-\frac{2m}{f_\pi^2}\langle\bar{\psi}\psi\rangle \tag{82}$$

where the pion decay constant in chiral limit follows as

$$f_\pi=\frac{\sqrt{N_c}M}{\sqrt{2}\pi}\left[\int_0^1 dx\int_0^\infty dk_\perp^2\frac{1}{k_\perp^2+M^2}\mathcal{F}(k)\mathcal{F}(P-k)\right]^{1/2}. \tag{83}$$

3. Vector ρ, ω channels

Each of the longitudinal and transverse vector gaplike equations can be shown to yield the same masses for ρ, ω. This is manifest if we use the spin averaged combination , that is $\frac{2}{3}$ of transverse mode equation (71) plus $\frac{1}{3}$ of longitudinal mode equation (72), with the result

$$1-\frac{2g_V}{3g_S}\left(1-\frac{m}{M}\right)=-\frac{4}{3}g_V(m_{\omega,\rho}^2+2M^2)\int_0^1 dx\int\frac{d^2k_\perp}{(2\pi)^3}\frac{1}{x\bar{x}m_{\omega,\rho}^2-(k_\perp^2+M^2)}\mathcal{F}(k)\mathcal{F}(P-k). \tag{84}$$

This remarkably simple prescription recovers the covariant gaplike equation for the vector mesons obtained in the covariant frame. With the explicit form factors, (84) is

$$1-\frac{2g_V}{3g_S}\left(1-\frac{m}{M}\right)=\frac{g_V}{3\pi^2}(m_{\omega,\rho}^2+2M^2)\int_0^1 dx\int_0^\infty dz\frac{z}{z^2-\frac{\rho^2}{4\lambda_V^2}\left(m_{\omega,\rho}^2-\frac{M^2}{x\bar{x}}\right)}[zF'(z)]^4. \tag{85}$$

In Fig. 8, the vector masses are shown in solid lines versus the current quark mass for different vector couplings g_V. The binding in the vector channels occurs only for a finite range of g_V. In the chiral limit with a constituent mass $M = 371.6$ MeV, the range is $0.382\times 2\pi^2\rho^2 < g_V < 1.562\times 2\pi^2\rho^2$ as shown in Fig. 9.

F. Physical mass spectrum

Our global results for the scalar and vector masses are summarized in the table

Model	m_{π^0} (MeV)	$m_{\pi^\pm}$ (MeV)	m_ω (MeV)	m_ρ (MeV)
ILM (this work)	135.0	135.0	780.0	780.0
PDG [61]	134.9766(6)	139.57018(35)	782.65 ± 0.12	775.26 ± 0.25

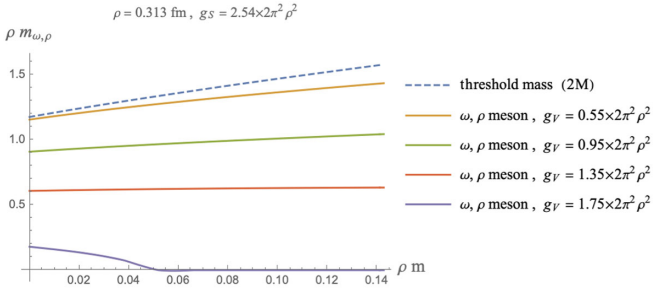

FIG. 8. Vector masses $m_{\omega,\rho}$ versus the current quark mass, in solid lines, for different vector couplings g_V. The dashed line is the $2M$ threshold in units of the instanton size ρ.

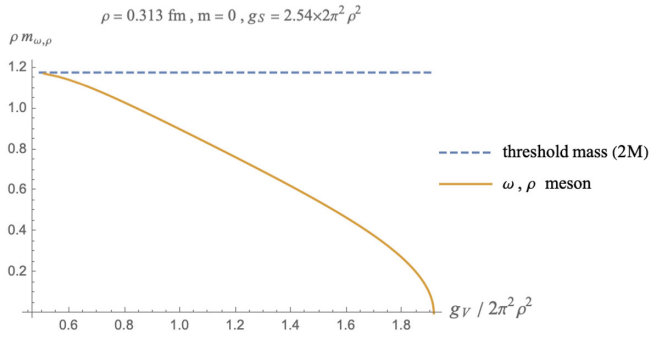

FIG. 9. Vector masses $m_{\omega,\rho}$ versus the vector coupling as a solid line, in units of the instanton size ρ. The dashed line is the $2M$ threshold.

where the parameters in the emergent 't Hooft action are fixed as

$$g_S = 2.540 \times 2\pi^2\rho^2 = 126.17\ \text{GeV}^{-2},$$
$$g_V = 0.531 \times 2\pi^2\rho^2 = 26.37\ \text{GeV}^{-2}, \tag{86}$$

with the current quark mass $m = 16.5$ MeV. This choice is commensurate with the standard $\rho = 0.313$ fm and $n_{I+\bar{I}} = 1\ \text{fm}^{-4}$ in the QCD instanton vacuum. The emergent constituent quark mass and the quark condensates are then

$$M = 398.2\ \text{MeV}, \qquad \langle\bar{\psi}\psi\rangle = (332.6\ \text{MeV})^3.$$

The determinantal mass which is a measure of the light quark hopping between the instanton and anti-instanton is found to be $m_{\text{det}} \approx 173.54$ MeV, which is close to the value of 103 MeV in [12,62]. The fixed parameters (86) translate to single and molecular induced couplings as

$$G_I = 248.34\ \text{GeV}^{-2}, \qquad G_{I\bar{I}} = 79.11\ \text{GeV}^{-2}.$$

The dimensionless hopping parameter $\xi = 40.25$ is fixed by (6).

V. LIGHT FRONT WAVE FUNCTIONS

The light front eigenstates (51) of the light front Hamiltonian follows from (52). In leading order in $1/N_c$, only the leading quark-antiquark Fock component is retained. The eigenstates consist of a scalar wave function times a spin-dependent matrix element encoding the spin-flavor quantum numbers. The scalar wave function fixes the size of the pertinent meson, together with the strength of its effective coupling to the quark-antiquark pair. It is normalized to 1,

$$\int_0^1 dx \int \frac{d^2k_\perp}{(2\pi)^3} \sum_{s_1,s_2} |\Phi_X^\lambda(x,k_\perp,s_1,s_2)|^2 = 1.$$

A. Light mesons light front wave functions

1. Scalar channels

$$\Phi_\sigma(x,k_\perp,s_1,s_2) = \frac{1}{\sqrt{N_c}}\left[\frac{C_\sigma}{\sqrt{2x\bar{x}\left(m_\sigma^2 - \frac{k_\perp^2+M^2}{x\bar{x}}\right)}}\sqrt{\mathcal{F}(k)\mathcal{F}(P-k)}\right]\bar{u}_{s_1}(k)v_{s_2}(P-k), \tag{87}$$

$$\Phi_{a_0}(x,k_\perp,s_1,s_2) = \frac{1}{\sqrt{N_c}}\left[\frac{C_{a_0}}{\sqrt{2x\bar{x}\left(m_{a_0}^2 - \frac{k_\perp^2+M^2}{x\bar{x}}\right)}}\sqrt{\mathcal{F}(k)\mathcal{F}(P-k)}\right]\bar{u}_{s_1}(k)\tau^a v_{s_2}(P-k). \tag{88}$$

The normalizations fix C_{σ,a_0} to

$$C_{\sigma,a_0} = -\left[2\int_0^1 dx \int \frac{d^2k_\perp}{(2\pi)^3}\frac{k_\perp^2+(x-\bar{x})^2M^2}{(x\bar{x}m_{\sigma,a_0}^2-k_\perp^2-M^2)^2}\mathcal{F}(k)\mathcal{F}(P-k)\right]^{-1/2}$$
$$= -\sqrt{2}\pi\left[\int_0^1 dx\int_0^\infty dzz\frac{x\bar{x}z^2+\frac{\rho^2}{4\lambda_S^2}(x-\bar{x})^2M^2}{\left(x\bar{x}z^2-\frac{\rho^2}{4\lambda_S^2}(x\bar{x}m_{\sigma,a_0}^2-M^2)\right)^2}(zF'(z))^4\right]^{-1/2}. \quad (89)$$

2. Pseudoscalar channels

$$\Phi_{\eta'}(x,k_\perp,s_1,s_2) = \frac{1}{\sqrt{N_c}}\left[\frac{C_{\eta'}}{\sqrt{2x\bar{x}}\left(m_{\eta'}^2-\frac{k_\perp^2+M^2}{x\bar{x}}\right)}\sqrt{\mathcal{F}(k)\mathcal{F}(P-k)}\right]\bar{u}_{s_1}(k)i\gamma^5 v_{s_2}(P-k), \quad (90)$$

$$\Phi_{\pi}(x,k_\perp,s_1,s_2) = \frac{1}{\sqrt{N_c}}\left[\frac{C_{\pi}}{\sqrt{2x\bar{x}}\left(m_{\pi}^2-\frac{k_\perp^2+M^2}{x\bar{x}}\right)}\sqrt{\mathcal{F}(k)\mathcal{F}(P-k)}\right]\bar{u}_{s_1}(k)i\gamma^5\tau^a v_{s_2}(P-k). \quad (91)$$

The normalizations fix $C_{\pi,\eta'}$ to

$$C_{\pi,\eta'} = -\left[2\int_0^1 dx \int \frac{d^2k_\perp}{(2\pi)^3}\frac{k_\perp^2+M^2}{(x\bar{x}m_{\pi,\eta'}^2-k_\perp^2-M^2)^2}\mathcal{F}(k)\mathcal{F}(P-k)\right]^{-1/2}$$
$$= -\sqrt{2}\pi\left[\int_0^1 dx\int_0^\infty dzz\frac{x\bar{x}z^2+\frac{\rho^2M^2}{4\lambda_S^2}}{\left(x\bar{x}z^2-\frac{\rho^2}{4\lambda_S^2}(x\bar{x}m_{\pi,\eta'}^2-M^2)\right)^2}(zF'(z))^4\right]^{-1/2}. \quad (92)$$

In chiral limit, C_π satisfies the Goldberger-Treiman relation.

$$\lim_{m_\pi\to 0} C_\pi = -\left[2\int_0^1 dx\int\frac{d^2k_\perp}{(2\pi)^3}\frac{1}{k_\perp^2+M^2}\mathcal{F}(k)\mathcal{F}(P-k)\right]^{-1/2} = -\frac{\sqrt{2N_c}M}{f_\pi}. \quad (93)$$

3. Vector channels

$$\Phi_{\omega}^{\lambda}(x,k_\perp,s_1,s_2) = \frac{1}{\sqrt{N_c}}\left[\frac{C_{\omega}}{\sqrt{2x\bar{x}}\left(m_{\omega}^2-\frac{k_\perp^2+M^2}{x\bar{x}}\right)}\sqrt{\mathcal{F}(k)\mathcal{F}(P-k)}\right]\epsilon_\lambda^\mu(P)\bar{u}_{s_1}(k)\gamma_\mu v_{s_2}(P-k), \quad (94)$$

$$\Phi_{\rho}^{\lambda}(x,k_\perp,s_1,s_2) = \frac{1}{\sqrt{N_c}}\left[\frac{C_{\rho}}{\sqrt{2x\bar{x}}\left(m_{\rho}^2-\frac{k_\perp^2+M^2}{x\bar{x}}\right)}\sqrt{\mathcal{F}(k)\mathcal{F}(P-k)}\right]\epsilon_\lambda^\mu(P)\bar{u}_{s_1}(k)\gamma_\mu\tau^a v_{s_2}(P-k). \quad (95)$$

The normalization yields different transverse C_{ω_T,ρ_T}

$$C_{\omega_T,\rho_T} = \left[2\int_0^1 dx\int\frac{d^2k_\perp}{(2\pi)^3}\frac{k_\perp^2+M^2-2x\bar{x}k_\perp^2}{(x\bar{x}m_{\omega,\rho}^2-k_\perp^2-M^2)^2}\mathcal{F}(k)\mathcal{F}(P-k)\right]^{-1/2}$$
$$= \sqrt{2}\pi\left[\int_0^1 dx\int_0^\infty dzx\bar{x}z\frac{(1-2x\bar{x})x\bar{x}z^2+\frac{\rho^2M^2}{4\lambda_V^2}}{\left(x\bar{x}z^2-\frac{\rho^2}{4\lambda_V^2}(x\bar{x}m_{\omega,\rho}^2-M^2)\right)^2}(zF'(z))^4\right]^{-1/2} \quad (96)$$

and longitudinal C_{ω_L,ρ_L}

$$C_{\omega_L,\rho_L} = \left[2\int_0^1 dx \int \frac{d^2k_\perp}{(2\pi)^3}\left(\frac{1}{m^2_{\omega,\rho}} + \frac{4x\bar{x}(k_\perp^2+M^2)}{(x\bar{x}m^2_{\omega,\rho} - k_\perp^2 - M^2)^2}\right)\mathcal{F}(k)\mathcal{F}(P-k)\right]^{-1/2}$$
$$= \sqrt{2}\pi\left[\int_0^1 dx \int_0^\infty dz x\bar{x}z\left(\frac{4\lambda_V^2}{\rho^2 m^2_{\omega,\rho}} + \frac{4x\bar{x}(x\bar{x}z^2 + \frac{\rho^2M^2}{4\lambda_V^2})}{\left(x\bar{x}z^2 - \frac{\rho^2}{4\lambda_V^2}(x\bar{x}m^2_{\omega,\rho} - M^2)\right)^2}\right)(zF'(z))^4\right]^{-1/2}. \quad (97)$$

More specifically, the violation of the Lorentz covariance in the light front transverse and longitudinal constants is captured by the identity

$$\frac{1}{3}\frac{1}{C^2_{\omega_L,\rho_L}} + \frac{2}{3}\frac{1}{C^2_{\omega_T,\rho_T}} = \frac{1}{C^2_{\omega,\rho}} + \frac{2}{3m^2_{\omega,\rho}}\int_0^1 dx \int \frac{d^2k_\perp}{(2\pi)^3}\mathcal{F}(k)\mathcal{F}(P-k) \quad (98)$$

which reflects on the irremediable loss of Lorentz symmetry on the light front. The spin average of the transverse and longitudinal constants is not equal to the covariant unpolarized constant $C^2_{\omega,\rho}$. The discrepancy is of order $C^2_{\omega,\rho}/(2\pi^2\rho^2 m^2_{\omega,\rho})$. Fortunately, our bookkeeping in $1/N_c$ suggests that

$$\frac{C^2_{\omega,\rho}}{g_{\omega,\rho}m^2_{\omega,\rho}} \sim \mathcal{O}(N_c^0)$$

as also observed in the context of effective models in [63,64]. As a result, the difference (98) is controlled by the molecular coupling

$$\frac{1}{3}\frac{1}{C^2_{\omega_L,\rho_L}} + \frac{2}{3}\frac{1}{C^2_{\omega_T,\rho_T}} \simeq \frac{1}{C^2_{\omega,\rho}}\left[1 + \mathcal{O}\left(\frac{g_V}{2\pi^2\rho^2}\right)\right] \quad (99)$$

which is parametrically subleading in the QCD instanton vacuum, thanks to its dilutenes. Recall that only the leading contributions g_V/g_S were retained in our bound state analysis both on the light front and in the covariant frame.

To summarize, the normalization constants in the LFWFs from the QCD instanton vacuum are

Model	$\lvert C_\sigma\rvert$	$\lvert C_\pi\rvert$	$\lvert C_{\omega_T,\rho_T}\rvert$	$\lvert C_{\omega_L,\rho_L}\rvert$	$\lvert C_{\omega,\rho}\rvert$
ILM	4.264	7.391	2.420	2.285	2.426

In the last three columns of the table, C_{ω_T,ρ_T} and C_{ω_L,ρ_L} follow from (96) and (97) using the light front analysis, while $C_{\omega,\rho}$ follows from the covariant analysis (see below). The covariance-violating term in (98) is numerically estimated to be 7.734×10^{-3} which is of order $\mathcal{O}(\frac{g_V}{2\pi^2\rho^2})$, hence parametrically small as we argued.

B. Bound state wave functions in covariant frame

The light front wave functions can also be obtained from the covariant formalism. In this section, we will show that their derivation from the covariant frame can be shown to agree with our derivation from the light front after a pertinent integration over the light front "energy." More specifically, in the covariant frame the Bethe-Salpeter (BS) wave functions are given by the residue of the 4-point Green's function, around the mass pole of each meson channel, or diagrammatically

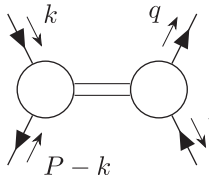

$$= \frac{-i\sum_\lambda \Psi_\lambda(q;P)\Psi^\dagger_\lambda(k;P)}{P^2 - m_X^2} \quad (100)$$

In the scalar and pseudoscalar channels, the BS wave functions are given by

$$\Psi_\sigma(k;P) = g_{\sigma qq}S(k)\sqrt{\mathcal{F}(k)}\sqrt{\mathcal{F}(P-k)}S(k-P),$$
$$\Psi_{a_0}(k;P) = g_{a_0qq}S(k)\sqrt{\mathcal{F}(k)}\tau^a\sqrt{\mathcal{F}(P-k)}S(k-P),$$
$$\Psi_{\eta'}(k;P) = g_{\eta'qq}S(k)\sqrt{\mathcal{F}(k)}i\gamma^5\sqrt{\mathcal{F}(P-k)}S(k-P),$$
$$\Psi_\pi(k;P) = g_{\pi qq}S(k)\sqrt{\mathcal{F}(k)}i\gamma^5\tau^a\sqrt{\mathcal{F}(P-k)}S(k-P), \quad (101)$$

where $S(k)$ is the quark propagator, while in the vector channels they are

$$\Psi_\omega(k;P) = g_{\omega qq}\epsilon^\mu_\lambda(P)S(k)\sqrt{\mathcal{F}(k)}\gamma_\mu\sqrt{\mathcal{F}(P-k)}S(k-P),$$
$$\Psi_\rho(k;P) = g_{\rho qq}\epsilon^\mu_\lambda(P)S(k)\sqrt{\mathcal{F}(k)}\gamma_\mu\tau^a\sqrt{\mathcal{F}(P-k)}S(k-P). \quad (102)$$

The effective quark-meson couplings g_{Xqq} follow as

$$g^2_{\sigma,a_0qq} = \left(\frac{\partial\Pi_{SS}}{\partial P^2}\right)^{-1}\Big|_{P^2=m^2_{\sigma,a_0}},$$
$$g^2_{\pi,\eta' qq} = \left(\frac{\partial\Pi_{PP}}{\partial P^2}\right)^{-1}\Big|_{P^2=m^2_{\pi,\eta'}},$$
$$g^2_{\omega,\rho qq} = \left(\frac{\partial\Pi_{VV}}{\partial P^2}\right)^{-1}\Big|_{P^2=m^2_{\omega,\rho}}. \tag{103}$$

The light front wave functions can be extracted from the covariant BS wave functions by integrating over the light front energy k^- of the BS wave functions and projecting out the bounded quark spins

$$\frac{1}{\sqrt{2x\bar{x}}}\Phi_X(x,k_\perp,s_1,s_2) = iP^+\int_{-\infty}^{\infty}\frac{dk^-}{2\pi}\frac{\bar{u}_{s_1}\gamma^+}{2k^+} \times \Psi_X(k;P)\frac{\gamma^+ v_{s_2}}{2(P^+-k^+)}\Big|_{k^+=xP^+}. \tag{104}$$

Alternatively, the integration of the BS kernel over the energy k^0 yields the equal-time wave function.

In the covariant frame, the normalization constant of each light front wave functions C_X is related to the effective quark-meson couplings g_{Xqq} in (103) as

$$g_{Xqq} = -\frac{C_X}{\sqrt{N_c}}. \tag{105}$$

Now we can compare the normalization constant derived from the light front formalism and from the covariant formalism. In the latter, the normalization follows from (105). More specifically, in the scalar and pseudoscalar channels the normalizations are readily shown to be the same. In the vector channels, the covariant normalization is the same for both longitudinal and transverse by Lorentz symmetry,

$$C_{\omega,\rho} = \left[\frac{4}{3}\int_0^1 dx\int\frac{d^2k_\perp}{(2\pi)^3}\frac{k_\perp^2+(1+2x\bar{x})M^2}{(x\bar{x}m^2_{\omega,\rho}-k_\perp^2-M^2)^2}\mathcal{F}(k)\mathcal{F}(P-k)\right]^{-1/2}$$
$$= \sqrt{3}\pi\left[\int_0^1 dx\int_0^\infty dz x\bar{x}z\frac{x\bar{x}z^2+(1+2x\bar{x})\frac{\rho^2M^2}{4\lambda_V^2}}{\left(x\bar{x}z^2-\frac{\rho^2}{4\lambda_V^2}(x\bar{x}m^2_{\omega,\rho}-M^2)\right)^2}(zF'(z))^4\right]^{-1/2}. \tag{106}$$

Using (98) with g_V/g_S parametrically small, (106) yields

$$C_{\omega,\rho} \simeq C_{\omega_T,\rho_T} \simeq C_{\omega_L,\rho_L}. \tag{107}$$

VI. PARTON DISTRIBUTION FUNCTIONS

In general, the partonic structure in a hadron can be studied using pertinent hadronic matrix elements. In leading twist, the only nontrivial partonic structure functions for spin-0 hadrons, are the parton density distributions. For spin-1 hadrons, the other two distributions, helicity and transversity, contribute in leading twist. These distribution functions are related to the Fourier transform of these matrix elements, which can be calculated using the light front wave functions.

A. Twist-2 parton distribution functions

Throughout, we will mainly focus on the twist-2 partonic structure functions, including the parton density functions for both spin-0 and spin-1 mesons, as well as the spin distribution functions (helicity and transversity) inside the spin-1 hadronic bound states.

1. Parton density distributions

Parton density distributions are defined as

$$q_X^\lambda(x) = \int_{-\infty}^{\infty}\frac{d\xi^-}{4\pi}e^{ixP^+\xi^-}\langle P\lambda|\bar{\psi}(0)\gamma^+W(0,\xi^-)\psi(\xi^-)|P\lambda\rangle = \int\frac{d^2k_\perp}{(2\pi)^3}\sum_{s,s'}|\Phi_X^\lambda(x,k,s,s')|^2 \tag{108}$$

for quarks, and

$$\bar{q}_X^\lambda(x) = \int_{-\infty}^{\infty}\frac{d\xi^-}{4\pi}e^{-ixP^+\xi^-}\langle P\lambda|\bar{\psi}(0)\gamma^+W(0,\xi^-)\psi(\xi^-)|P\lambda\rangle = \int\frac{d^2k_\perp}{(2\pi)^3}\sum_{s,s'}|\Phi_X^\lambda(\bar{x},k,s,s')|^2 \tag{109}$$

for the antiquarks, where

$$W(\xi^-,0)=\exp\left[-ig\int_0^{\xi^-}d\eta^- A^+(\eta^-)\right]$$

is a lightlike gauge link. In the case of the meson PDFs, the quark and antiquark distributions are also related by spin symmetry

$$\bar{q}_X(x)=q_{\bar{X}}(x)=q_X(1-x)=\bar{q}_{\bar{X}}(1-x).$$

For spin-1 meson, the quark distributions for different polarizations are related also by spin symmetry

$$q_X^+(x)=q_X^-(x)=q_X^T(x),\qquad q_X^0(x)=q_X^L(x).$$

Scalar channels: the σ PDF follws as

$$\begin{aligned}q_\sigma(x)&=2C_\sigma^2\int_0^1 dx\int\frac{d^2k_\perp}{(2\pi)^3}\frac{k_\perp^2+(x-\bar{x})^2M^2}{(x\bar{x}m_\sigma^2-k_\perp^2-M^2)^2}\mathcal{F}(k)\mathcal{F}(P-k)\\&=\frac{C_\sigma^2}{2\pi^2}x\bar{x}\int_0^\infty dzz\frac{x\bar{x}z^2+(x-\bar{x})^2\frac{\rho^2M^2}{4\lambda_S^2}}{\left(x\bar{x}z^2-\frac{\rho^2}{4\lambda_S^2}(x\bar{x}m_\sigma^2-M^2)\right)^2}(zF'(z))^4.\end{aligned}\tag{110}$$

Pseudoscalar channels: the pion and eta prime PDF follows as

$$\begin{aligned}q_{\pi,\eta'}(x)&=2C_\pi^2\int\frac{d^2k_\perp}{(2\pi)^3}\frac{k_\perp^2+M^2}{(x\bar{x}m_\pi^2-k_\perp^2-M^2)^2}\mathcal{F}(k)\mathcal{F}(P-k)\\&=\frac{C_{\pi,\eta'}^2}{2\pi^2}x\bar{x}\int_0^\infty dzz\frac{x\bar{x}z^2+\frac{\rho^2M^2}{4\lambda_S^2}}{\left(x\bar{x}z^2-\frac{\rho^2}{4\lambda_S^2}(x\bar{x}m_{\pi,\eta'}^2-M^2)\right)^2}(zF'(z))^4.\end{aligned}\tag{111}$$

Vector channels: the vector PDF for the transverse mode can be evaluated as

$$q_{\omega,\rho}^T(x)=2C_{\omega_T,\rho_T}^2\int\frac{d^2k_\perp}{(2\pi)^3}\frac{k_\perp^2+M^2-2x\bar{x}k_\perp^2}{(x\bar{x}m_{\omega,\rho}^2-k_\perp^2-M^2)^2}\mathcal{F}(k)\mathcal{F}(P-k).\tag{112}$$

The PDF for the longitudinal mode can be evaluated as

$$q_{\omega,\rho}^L(x)=2C_{\omega_L,\rho_L}^2\int\frac{d^2k_\perp}{(2\pi)^3}\left[\frac{1}{m_{\omega,\rho}^2}+\frac{4x\bar{x}(k_\perp^2+M^2)}{(x\bar{x}m_{\omega,\rho}^2-k_\perp^2-M^2)^2}\right]\mathcal{F}(k)\mathcal{F}(P-k).\tag{113}$$

As we noted earlier, the difference between the longitudinal and transverse normalizations in QCD instanton vacuum on the light front is controlled by the ratio g_V/g_S which is parametrically small. Recall that in our bookkeeping analysis in leading order in $1/N_c$ only the leading g_V/g_S are also to be retained in the dilute limit. With this in mind, in the QCD instanton vacuum we obtain

$$q_{\omega,\rho}^T(x)\simeq\frac{C_{\omega,\rho}^2}{2\pi^2}x\bar{x}\int_0^\infty dzz\frac{(1-2x\bar{x})x\bar{x}z^2+\frac{\rho^2M^2}{4\lambda_V^2}}{\left(x\bar{x}z^2-\frac{\rho^2}{4\lambda_V^2}(x\bar{x}m_{\omega,\rho}^2-M^2)\right)^2}(zF'(z))^4,\tag{114}$$

$$q_{\omega_L,\rho_L}^L(x)\simeq\frac{C_{\omega,\rho}^2}{2\pi^2}x\bar{x}\int_0^\infty dzz\frac{4x\bar{x}(x\bar{x}z^2+\frac{\rho^2M^2}{4\lambda_V^2})}{\left(x\bar{x}z^2-\frac{\rho^2}{4\lambda_X^2}(x\bar{x}m_{\omega,\rho}^2-M^2)\right)^2}(zF'(z))^4+\mathcal{O}\left(\frac{g_V}{2\pi^2\rho^2}x\bar{x}\right).\tag{115}$$

The polarization average over transverse mode and longitudinal mode yields the unpolarized PDF:

$$q_{\omega,\rho}(x) = \frac{2}{3} q^T_{\omega,\rho}(x) + \frac{1}{3} q^L_{\omega,\rho}(x)$$
$$\simeq \frac{4}{3} C^2_{\omega,\rho} \int \frac{d^2k_\perp}{(2\pi)^3} \frac{k^2_\perp + (1+2x\bar{x})M^2}{(x\bar{x}m^2_{\omega,\rho} - k^2_\perp - M^2)^2} \mathcal{F}(k)\mathcal{F}(P-k)$$
$$= \frac{C^2_{\omega,\rho}}{3\pi^2} x\bar{x} \int_0^\infty dzz \frac{x\bar{x}z^2 + (1+2x\bar{x})\frac{\rho^2 M^2}{4\lambda_V^2}}{\left(x\bar{x}z^2 - \frac{\rho^2}{4\lambda_M^2}(x\bar{x}m^2_{\omega,\rho} - M^2)\right)^2} (zF'(z))^4. \quad (116)$$

In Fig. 10 we show our results for the vector mesons PDFs versus x in the QCD instanton vacuum for $\rho = 0.313$ fm, $m_{\omega,\rho} = 780$ MeV and a constituent mass $M = 398.2$ MeV. The transverse PDF for the vectors is in solid green, the longitudinal PDF for the vectors is in solid red, and the unpolarized PDF in dashed blue. Note the small differences due to the parametrically small value of g_V/g_S, with the exception of the end points for the longitudinal polarization. The unpolarized PDF is identical to that from the covariant analysis. In Fig. 11 we show the parton density functions versus parton-x, for the sigma meson in solid green, the pion in solid blue, and the rho meson in solid red in the chiral limit. In this limit, the constituent mass is $M = 372.3$ MeV.

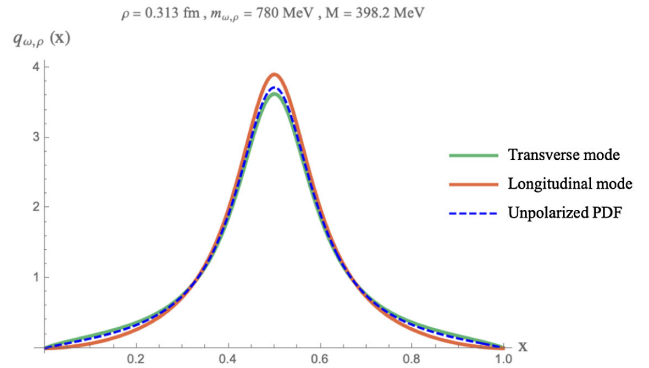

FIG. 10. Vector mesons PDFs versus parton-x: transverse polarization (solid green), longitudinal polarization (solid red). and unpolarized (dashed blue).

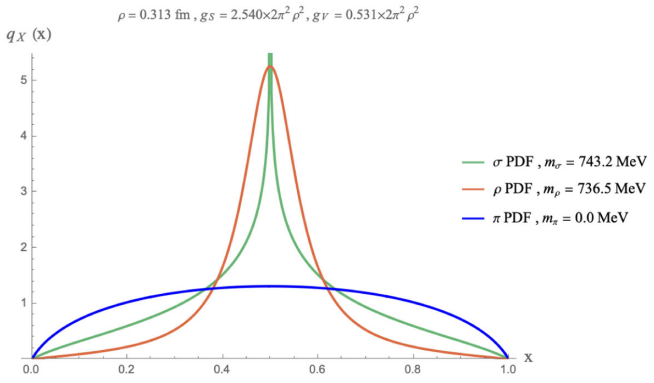

FIG. 11. Parton density functions in the chiral limit.

2. Spin-dependent parton distributions

For mesons with spin, we can also probe the parton distribution in a polarized hadron. In the case of spin-1 mesons, the spin-dependent parton distribution can be described by the helicity distribution functions. For quarks, the helicity distribution is given by

$$\Delta q^\lambda_X(x) = \int_{-\infty}^{\infty} \frac{d\xi^-}{4\pi} e^{ixP^+\xi^-} \langle P\lambda|\bar{\psi}(0)\gamma^+\gamma^5 W(0,\xi^-)\psi(\xi^-)|P\lambda\rangle$$
$$= \int \frac{d^2k_\perp}{(2\pi)^3} \sum_{s,s'} s|\Phi^\lambda_X(x,k,s,s')|^2 \quad (117)$$

and for the antiquarks, it is given by

$$\Delta\bar{q}^\lambda_X(x) = \int_{-\infty}^{\infty} \frac{d\xi^-}{4\pi} e^{-ixP^+\xi^-} \langle P\lambda|\bar{\psi}(0)\gamma^+\gamma^5 W(0,\xi^-)\psi(\xi^-)|P\lambda\rangle$$
$$= \int \frac{d^2k_\perp}{(2\pi)^3} \sum_{s,s'} s'|\Phi^\lambda_X(\bar{x},k,s,s')|^2. \quad (118)$$

Charge symmetry implies that the helicity distributions for the quarks and antiquarks are tied,

$$\Delta\bar{q}_X(x) = \Delta q_{\bar{X}}(x) = \Delta q_X(1-x) = \Delta\bar{q}_{\bar{X}}(1-x).$$

The quark helicity distributions for different polarizations are also related by spin symmetry,

$$\Delta q^+_X(x) = -\Delta q^-_X(x) \qquad \Delta q^0_X(x) = 0.$$

Due to the charge symmetry, the quark and antiquark should contribute to the meson helicity equally. Therefore, the helicity distribution in the longitudinal state is zero. Only the transverse modes have nontrivial helicity parton distribution, hence

$$\Delta q^{\pm}_{\omega,\rho}(x) = \pm\frac{C^2_{\omega,\rho}}{2}\int\frac{d^2k_\perp}{(2\pi)^3}\frac{xk^2_\perp + M^2}{(x\bar{x}m^2_{\omega,\rho} - k^2_\perp - M^2)^2}\mathcal{F}(k)\mathcal{F}(P-k)$$
$$= \pm\frac{C^2_{\omega,\rho}}{4\pi^2}\int_{\frac{\rho M}{2\lambda_M\sqrt{x\bar{x}}}}^{\infty} dz z\frac{xz^2 + \frac{\rho^2M^2}{4x\lambda^2_M}}{\left(\frac{\rho^2 m^2_{\omega,\rho}}{4\lambda^2_M} - z^2\right)^2}(zF'(z))^4. \quad (119)$$

The result satisfies the helicity sum rule,

$$\int_0^1 dx[\Delta q^{\lambda}_{\omega,\rho}(x) + \Delta q^{\lambda}_{\omega,\rho}(1-x)] = \lambda. \quad (120)$$

As expected, the quark and antiquark contribute to the meson helicity equally.

In Fig. 12 we show the parton helicity polarization in a vector meson with transverse polarization $\lambda = +$ versus parton-x, in the QCD instanton vacuum. The quark helicity polarization is shown in solid blue, and the antiquark helicity polarization is shown in solid brown. The helicity distributions are comparable away from the end points.

VII. MESON DISTRIBUTION AMPLITUDES

In general, the distribution amplitudes are the leading twist transition matrix elements between a pertinent hadron and the vacuum. Throughout, the DAs will be normalized to 1.

A. Pseudoscalar meson distribution amplitude

The twist-2 DA of the pseudoscalar meson is defined as

$$\langle 0|\bar{\psi}(0)\gamma^+\gamma^5\frac{\tau^a}{\sqrt{2}}W(0,\xi^-)\psi(\xi^-)|\pi^a(P)\rangle$$
$$= if_\pi P^+\int_0^1 dx e^{-ixP^+\xi^-}\phi^A_\pi(x) \quad (121)$$

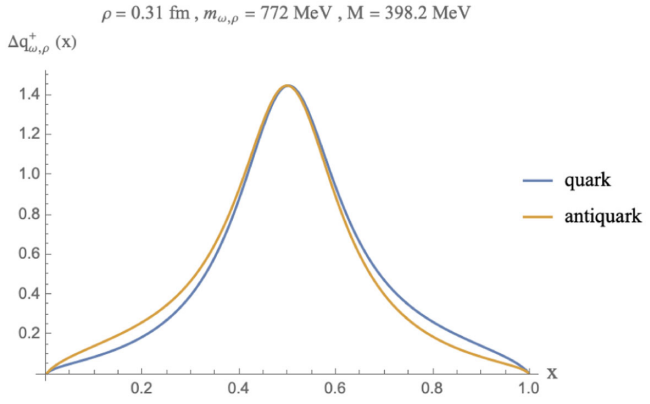

FIG. 12. Helicity distribution function for the quark (solid blue) and the antiquark (solid brown) in a +polarized vector meson, versus parton-x.

where the pion decay constant is defined as

$$\langle 0|\bar{\psi}\gamma^\mu\gamma^5\frac{\tau^a}{\sqrt{2}}\psi|\pi^a(P)\rangle = if_\pi P^\mu. \quad (122)$$

For $\pi^\mp$, we have $\tau^\pm = (\tau^1 \pm i\tau^2)/\sqrt{2}$ and for π^0, we have τ^3. Hence, the twist-2 DA of the pseudoscalar meson can be expressed in terms of the light front pion wave function

$$\phi^A_\pi(x) = 4\frac{\sqrt{2N_c}M}{f_\pi}\int\frac{d^2k_\perp}{(2\pi)^3}\frac{\phi_\pi(x,k_\perp)}{\sqrt{2x\bar{x}}}[x\mathcal{F}(P-k) + \bar{x}\mathcal{F}(k)]. \quad (123)$$

Similarly, the decay constant can also be written in terms of the light front wave function,

$$f_\pi = 4\sqrt{2N_c}M\int_0^1 dx$$
$$\times\int\frac{d^2k_\perp}{(2\pi)^3}\frac{\phi_\pi(x,k_\perp)}{\sqrt{2x\bar{x}}}[x\mathcal{F}(P-k) + \bar{x}\mathcal{F}(k)]. \quad (124)$$

To enforce axial current conservation, it is natural to assume that

$$x\mathcal{F}(P-k) + \bar{x}\mathcal{F}(k) \approx \mathcal{F}\left(\frac{k_\perp}{2\lambda_S\sqrt{x\bar{x}}}\right).$$

Thus, the pion DA with the quark form factor is

$$\phi^A_\pi(x) = \frac{\sqrt{2N_c}M}{2\pi^2 f_\pi}C_\pi x\bar{x}\int_0^\infty$$
$$\times dz\frac{z}{\frac{\rho^2}{4\lambda^2_S}(x\bar{x}m^2_\pi - M^2) - x\bar{x}z^2}(zF'(z))^4 \quad (125)$$

and the pion decay constant with the quark form factor is

$$f_\pi = \frac{\sqrt{2N_c}M}{2\pi^2}C_\pi\int_0^1 dx\int_0^\infty$$
$$\times dzx\bar{x}z\frac{1}{\frac{\rho^2}{4\lambda^2_S}(x\bar{x}m^2_\pi - M^2) - x\bar{x}z^2}(zF'(z))^4. \quad (126)$$

The pion (axial) DA $\phi^A(x)$ is normalized to 1,

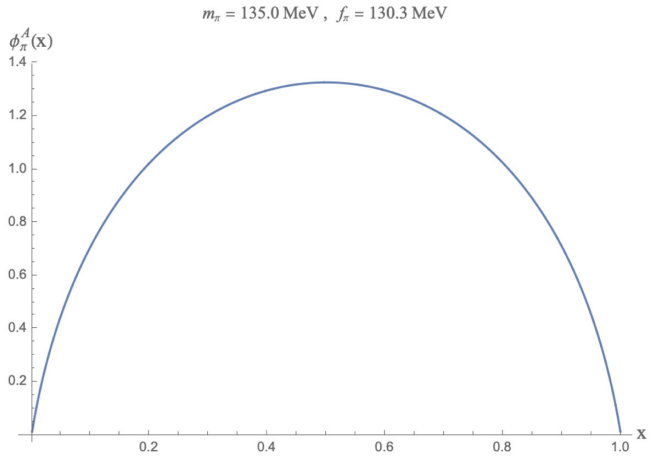

FIG. 13. The unevolved pion DA versus parton-x at low resolution, in the QCD instanton vacuum.

$$\int_0^1 dx\phi_\pi^A(x) = 1. \tag{127}$$

In Fig. 13 we show the unevolved pion DA versus parton-x in the QCD instanton vacuum at low resolution. Our result for the evolved pion DA is shown in Fig. 14 in solid blue, using the NLO ERBL equation to a scale of $\mu = 2$ GeV. Our result is compared to the QCD asymptotic result in dashed black, the lattice calculation from the RQCD Collaboration [65] in shaded-purple, and the Dyson-Schwinger equation (DSE) in solid green [66]. The empirical pion DA data points in brown are extracted from π^- into dijets via diffractive dissociation with invariant dijet mass 6 GeV [67], with the normalization discussed in [68].

B. Longitudinally polarized vector meson distribution amplitude

The leading twist DA of the longitudinally polarized vector meson is defined as

$$\langle 0|\bar{\psi}(0)\gamma^+\frac{1}{\sqrt{2}}W(0,\xi^-)\psi(\xi^-)|\omega(\lambda,P)\rangle = f_\omega m_\omega \epsilon_\lambda^+(P)\int_0^1 dx e^{-ixP^+\xi^-}\phi_\omega^V(x), \tag{128}$$

$$\langle 0|\bar{\psi}(0)\gamma^+\frac{\tau^a}{\sqrt{2}}W(0,\xi^-)\psi(\xi^-)|\rho(\lambda,P)\rangle = f_\rho m_\rho \epsilon_\lambda^+(P)\int_0^1 dx e^{-ixP^+\xi^-}\phi_\rho^V(x), \tag{129}$$

where the vector meson decay constants are set by

$$\langle 0|\bar{\psi}\gamma^\mu\frac{1}{\sqrt{2}}\psi|\omega(P,\lambda)\rangle = f_\omega m_\omega \epsilon_\lambda^\mu(P), \tag{130}$$

$$\langle 0|\bar{\psi}\gamma^\mu\frac{\tau^a}{\sqrt{2}}\psi|\rho^a(P,\lambda)\rangle = f_\rho m_\rho \epsilon_\lambda^\mu(P). \tag{131}$$

The longitudinal meson distribution amplitude is related to the light front wave function through

$$\phi_{\omega,\rho}^V(x) = -\frac{2\sqrt{2N_c}}{f_{\omega,\rho}m_{\omega,\rho}}\int\frac{d^2k_\perp}{(2\pi)^3}\frac{\phi_{\omega,\rho}(x,k_\perp)}{\sqrt{2x\bar{x}}}2[x\bar{x}m^2 + k_\perp^2 + M(k)M(P-k)]. \tag{132}$$

To avoid the nonlocal effect of the emergent interactions [38,69,70], we will limit the analysis to the longitudinally polarized vector meson. We recall that the nonlocal vertices in this case are purely transverse, hence blind to the

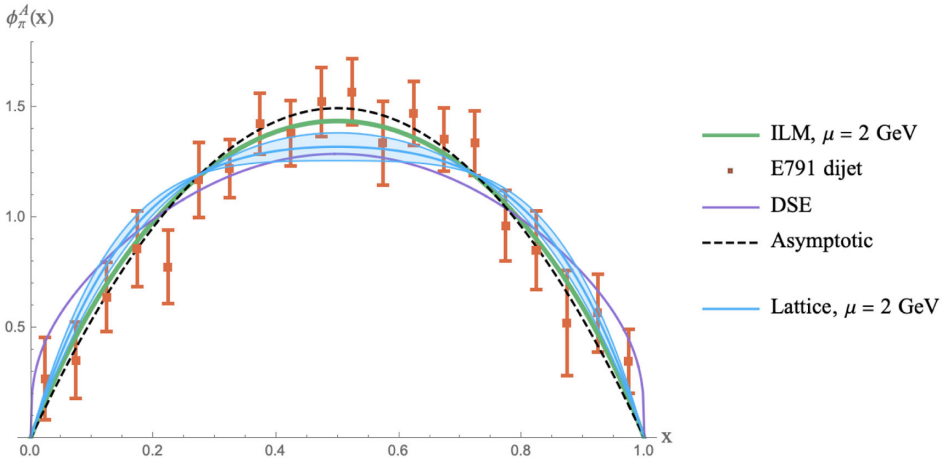

FIG. 14. The evolved pion DA using the NLO ERBL equation to $\mu = 2$ GeV (solid green), compared with the lattice calculation (RQCD) (shaded blue) [65], Dyson-Schwinger result [66] (solid purple), and the asymptotic QCD result (dashed black). The experimental data points (red squared points) are extracted from π^- into dijets via diffractive dissociation with invariant dijet mass 6 GeV [67] and normalized in [68].

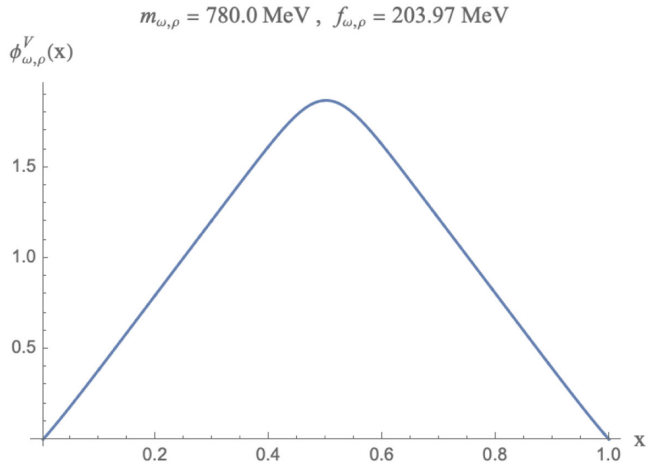

FIG. 15. Unevolved longitudinal vector DA in the QCD instanton vacuum at low resolution with $\mu \sim 1/2\rho$.

longitudinal polarization through minimal substitution. With this in mind, the longitudinally polarized vector meson contribution to the decay amplitude is

$$f_{\omega,\rho} = -\frac{2\sqrt{2N_c}}{m_{\omega,\rho}} \int_0^1 dx \int \frac{d^2k_\perp}{(2\pi)^3} \frac{\phi_{\omega,\rho}(x,k_\perp)}{\sqrt{2x\bar{x}}} 2[x\bar{x}m^2_{\omega,\rho} + k^2_\perp + M^2\mathcal{F}(k)\mathcal{F}(P-k)]. \quad (133)$$

To recover the Lorentz covariance and enforce current conservation, we remove the Lorentz violating term by approximating

$$x\bar{x}m^2_{\omega,\rho} + k^2_\perp + M(k)M(P-k) \approx 2(k^2_\perp + M^2)\mathcal{F}^2\left(\frac{k_\perp}{2\lambda_V\sqrt{x\bar{x}}}\right)$$

which amounts to

$$f_{\omega,\rho} = -\frac{\sqrt{2N_c}}{4\pi^2 m_{\omega,\rho}} C_{\omega_L,\rho_L} \frac{4\lambda_V^2}{\rho^2} \int_0^1 dx \int_0^\infty dz z \times \frac{4x\bar{x}\left[\frac{\rho^2M^2}{4\lambda_V^2} + x\bar{x}z^2\right]}{\left[\frac{\rho^2}{4\lambda_V^2}(x\bar{x}m^2_{\omega,\rho} - M^2) - x\bar{x}z^2\right]} (zF'(z))^6 \quad (134)$$

hence the longitudinally polarized vector meson DA

$$\phi^V_{\omega,\rho}(x) = -\frac{\sqrt{2N_c}}{4\pi^2 f_{\omega,\rho} m_{\omega,\rho}} C_{\omega_L,\rho_L} \frac{4\lambda_V^2}{\rho^2} \int_0^\infty dz z \times \frac{4x\bar{x}\left[\frac{\rho^2M^2}{4\lambda_V^2} + x\bar{x}z^2\right]}{\left[\frac{\rho^2}{4\lambda_V^2}(x\bar{x}m^2_{\omega,\rho} - M^2) - x\bar{x}z^2\right]} (zF'(z))^6. \quad (135)$$

In Fig. 15 we show the unevolved longitudinal vector meson DA versus parton-x in the QCD instanton vacuum at low resolution $\mu \sim 1/2\rho$. The evolved DA using NLO ERBL to $\mu = 2$ GeV is shown in Fig. 16 as solid blue, and compared to the QCD asymptotic result $6x\bar{x}$ as dashed black, and the QCD sum rule result from [71] as filled purple. The lattice results from [72] are in filled brown, and the lattice from [73] are in filled green.

C. Transversely polarized vector meson distribution amplitude

The general twist-2 DAs for the transversely polarized vector mesons are

$$\langle 0|\bar{\psi}(0) i\gamma^+\gamma^i_\perp \frac{1}{\sqrt{2}} W(0,\xi^-)\psi(\xi^-)|\omega(\lambda,P)\rangle = -if^T_\omega P^+ \epsilon^i_\lambda(P) \int_0^1 dx e^{-ixP^+\xi^-} \phi^T_\omega(x), \quad (136)$$

$$\langle 0|\bar{\psi}(0) i\gamma^+\gamma^i_\perp \frac{\tau^a}{\sqrt{2}} W(0,\xi^-)\psi(\xi^-)|\rho(\lambda,P)\rangle = -if^T_\omega P^+ \epsilon^i_\lambda(P) \int_0^1 dx e^{-ixP^+\xi^-} \phi^T_\rho(x), \quad (137)$$

where the transverse decay constants are defined as

$$\langle 0|\bar{\psi}\sigma^{\mu\nu}\frac{1}{\sqrt{2}}\psi|\omega(P,\lambda)\rangle = if^T_\omega(\epsilon^\mu_\lambda P^\nu - \epsilon^\nu_\lambda P^\mu), \quad (138)$$

$$\langle 0|\bar{\psi}\sigma^{\mu\nu}\frac{\tau^a}{\sqrt{2}}\psi|\rho^a(P,\lambda)\rangle = if^T_\rho(\epsilon^\mu_\lambda P^\nu - \epsilon^\nu_\lambda P^\mu). \quad (139)$$

Using the light front wave functions, we obtain

$$\phi^T_{\omega,\rho}(x) = -4\frac{\sqrt{2N_c}M}{f^T_{\omega,\rho}} \int \frac{d^2k_\perp}{(2\pi)^3} \frac{\phi_{\omega,\rho}(x,k_\perp)}{\sqrt{2x\bar{x}}} [x\mathcal{F}(P-k) + \bar{x}\mathcal{F}(k)] \quad (140)$$

with the vector meson decay constant

$$f^T_{\omega,\rho} = -4\sqrt{2N_c}M \int_0^1 dx \int \frac{d^2k_\perp}{(2\pi)^3} \frac{\phi_{\omega,\rho}(x,k_\perp)}{\sqrt{2x\bar{x}}} [x\mathcal{F}(P-k) + \bar{x}\mathcal{F}(k)] \quad (141)$$

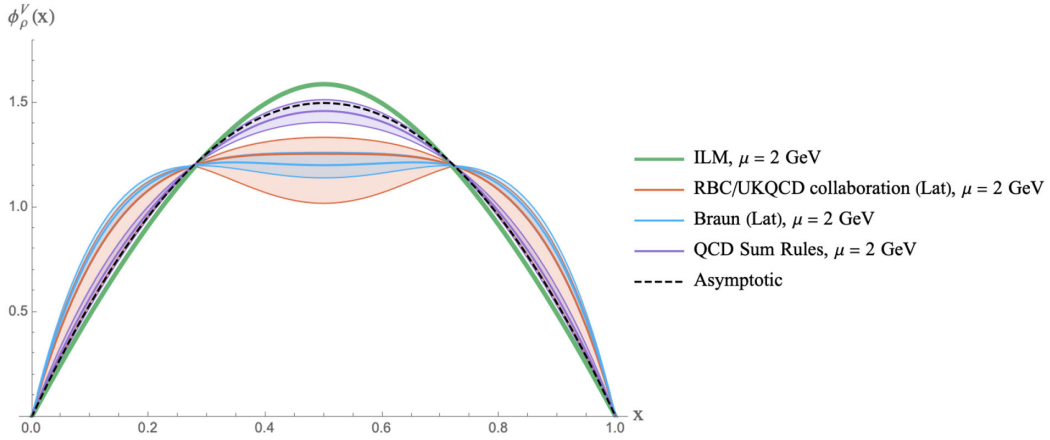

FIG. 16. Evolved longitudinal ρ DA to $\mu = 2$ GeV in solid green, compared with the lattice in RBC/UKQCD Collaboration [72] in filled red and the lattice [73] in filled blue. The QCD asymptotic result of $6x\bar{x}$ is in dashed black and the QCD sum result [71] is in filled purple.

following from the normalization of the DA to 1. Again, to enforce current conservation we approximate

$$x\mathcal{F}(P-k) + \bar{x}\mathcal{F}(k) \approx \mathcal{F}\left(\frac{k_\perp}{2\lambda_V\sqrt{x\bar{x}}}\right)$$

which yields the DA

$$\phi^T_{\omega,\rho}(x) = -\frac{\sqrt{2N_c}M}{2\pi^2 f^T_{\omega,\rho}} C_{\omega_T,\rho_T} \int_0^\infty dz x\bar{x}z \frac{1}{\frac{\rho^2}{4\lambda_V^2}(x\bar{x}m^2_{\omega,\rho} - M^2) - x\bar{x}z^2} (zF'(z))^4 \tag{142}$$

and the transverse vector meson decay constant

$$f^T_{\omega,\rho} = -\frac{\sqrt{2N_c}M}{2\pi^2} C_{\omega_T,\rho_T} \int_0^1 dx \int_0^\infty dz x\bar{x}z \frac{1}{\frac{\rho^2}{4\lambda_V^2}(x\bar{x}m^2_{\omega,\rho} - M^2) - x\bar{x}z^2} (zF'(z))^4. \tag{143}$$

The transverse decay constant $f^T_{\omega,\rho}$ is scale dependent due to the nonzero anomalous dimension of the tensor current [74],

$$f^T_{\omega,\rho}(\mu) = f^T_{\omega,\rho}(\mu_0)\left(\frac{\alpha_s(\mu)}{\alpha_s(\mu_0)}\right)^{C_F/\beta_0} \tag{144}$$

using the one-loop perturbative QCD result, with $C_F = \frac{N_c^2-1}{2N_c}$ and $\beta_0 = 11 - \frac{2}{3}N_f$.

In Fig. 17 we show the unevolved transverse DA versus parton-x, in the QCD instanton vacuum at low resolution $\mu \sim 1/2\rho$. The evolved transverse DA using NLO ERBL to $\mu = 2$ GeV is shown in Fig. 18 in solid blue, and compared to the QCD asymptotic result $6x\bar{x}$ in dashed black. The lattice results at $\mu = 2$ GeV [73] are shown in filled brown, and the QCD sum rule result also at $\mu = 2$ GeV [75] are shown in filled purple.

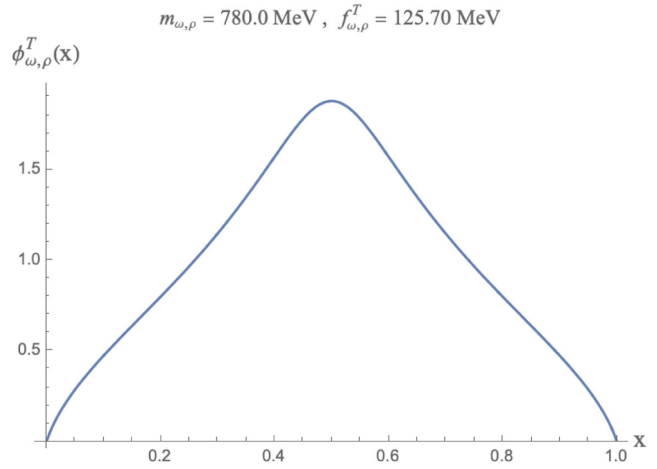

FIG. 17. Unevolved transverse DA for a vector meson in the QCD instanton vacuum at a resolutio $\mu \sim 1/2\rho$.

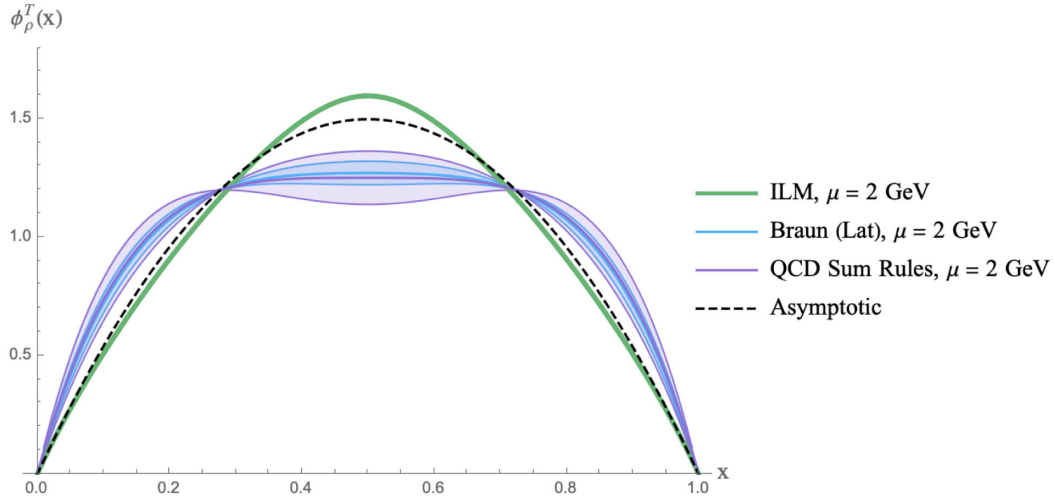

FIG. 18. Evolved transverse DA for the rho meson at $\mu = 2$ GeV in solid green, and compared with the lattice result at $\mu = 2$ GeV [73] in filled blue and the QCD sum rule result also at $\mu = 2$ GeV [75] in filled purple.

D. End-point behavior and ERBL evolution

The comparison between our results in the QCD instanton vacuum at low resolution $\mu = 0.313$ GeV, and the data as well as the lattice results at higher resolution at $\mu = 2$ GeV, required the use of the Efremov-Radyushkin-Brodsky-Lepage (ERBL) evolution of the DA, briefly reviewed in Appendix E. Recall that the anomalous dimensions for ϕ_π^A and $\phi_{\omega,\rho}^V$ are the same (conserved currents, but only in the chiral limit for the former), while the anomalous dimension for $\phi_{\omega,\rho}^T$ is different due to the running of the quark tensor current. We now focus on the behavior of the end points for the pseudoscalar and vector DAs.

In Fig. 19 we show the twist-2 pion DA versus parton-x in the QCD instanton vacuum at low resolution with $\mu = 0.313$ GeV in solid green, the evolved DA with $\mu = 2$ GeV in solid red, and the QCD asymptotic result $6x\bar{x}$ in dashed black. We note that $\phi_\pi^A(x \to 1, \mu = 0.313\ \text{GeV}) \sim 10.56(1-x)^{0.959}$ near the end point, and asymptotes the QCD result at infinite resolution.

In Fig. 20 we show the longitudinally polarized vector twist-2 DA versus parton-x, in the QCD instanton vacuum at low resolution with $\mu = 0.313$ GeV in solid green, the evolved DA with $\mu = 2$ GeV in solid red, and the QCD asymptotic result $6x\bar{x}$ in dashed black. The longitudinal vector DA at the end point scales as $\phi_\rho^V(x \to 1, \mu = 0.313\ \text{GeV}) \sim 3.68(1-x)^{1.0067}$ asymptotically. The evolution broadens somewhat the DA.

In Fig. 21 we show the transversely polarized vector twist-2 DA versus parton-x, in the QCD instanton vacuum at low resolution with $\mu = 0.313$ GeV in solid green, the evolved DA with $\mu = 2$ GeV in solid red, and the QCD asymptotic result $6x\bar{x}$ in dashed black. The end point behavior of the transversely polarized vector twist-2 distribution amplitude scales as $\phi_\rho^T(x \to 1, \mu = 0.313\ \text{GeV}) \sim 6.37(1-x)^{0.9402}$ at the initial scale. The evolution depletes the DA near the end points, by increasing the power and eventually the DA approaches its asymptotic form.

E. Meson decay constants

In the QCD instanton vacuum with the fixed parameters detailed above, we obtain for the pseudoscalar and vector decay constants,

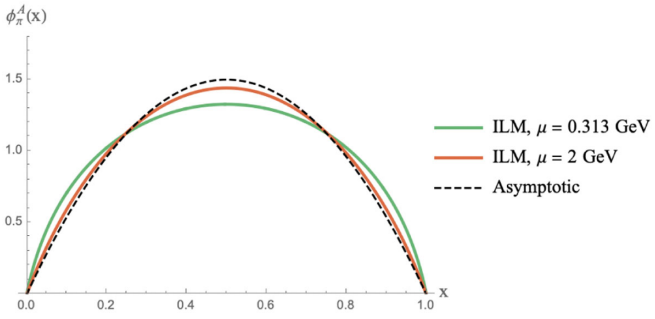

FIG. 19. The pion twist-2 distribution amplitude at $\mu = 0.313$ GeV, $\mu = 2$ GeV, and $\mu = \infty$ (asymptotic form).

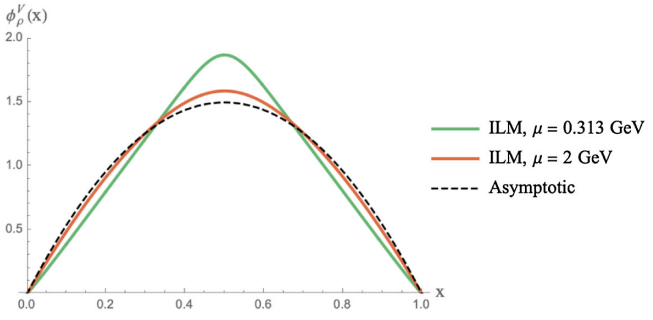

FIG. 20. The longitudinally polarized vector twist-2 distribution amplitude at $\mu = 0.313$ GeV, $\mu = 2$ GeV, and $\mu = \infty$ (asymptotic form).

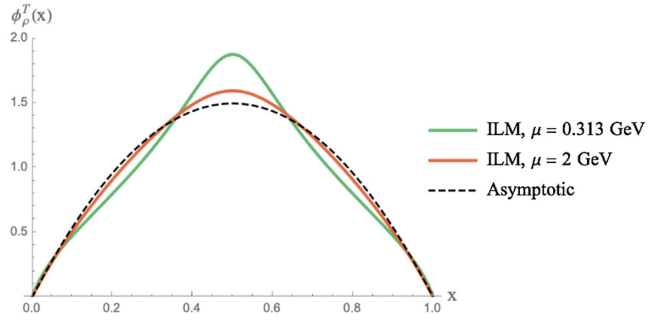

FIG. 21. The transversely polarized vector twist-2 distribution amplitude at $\mu = 0.313$ GeV, $\mu = 2$ GeV, and $\mu = \infty$ (asymptotic form).

$$f_\pi = 130.3 \text{ MeV}, \qquad f_\rho = 203.97 \text{ MeV},$$
$$f_\rho^T = 125.70 \text{ MeV}, \qquad f_\rho^T/f_\rho = 0.6163.$$

Cata and Mateu [76] have argued that in the large N_c limit $f_\rho^T/f_\rho = 1/\sqrt{2} \simeq 0.707$. Our result is consistent with tis ratio. Our results are compared with the lattice calculations [73], and the values quoted by the Particle Data Group [77] in the table below. The transverse ρ decay constant f_ρ^T is evolved to 2 GeV starting from 0.313 GeV using (144) when compared with the lattice. We display the results at $Q = 2$ GeV.

	f_π (MeV)	f_ρ (MeV)	f_ρ^T (MeV)	f_ρ^T/f_ρ
ILM (this work)	130.3	203.97	92.48	0.453
Lattice (2 GeV) [73]	⋯	199(4)(1)	124(4)(1)	0.629(8)
PDG (exp) [77]	130.3 ± 0.3	210 ± 4	⋯	⋯

VIII. MESON ELECTROMAGNETIC FORM FACTORS

The electromagnetic form factor $F_X(Q^2)$ in hadron-X is given by the transition matrix element of the EM current

$$J^\mu_{\rm EM} = \sum_f Q_f \bar\psi_f \gamma^\mu \psi_f; \tag{145}$$

(i) spin-0 meson electromagnetic form factor:

$$\langle X(P')|J^\mu_{\rm EM}|X(P)\rangle = F_X(Q^2)(P+P')^\mu, \tag{146}$$

(ii) spin-1 meson electromagnetic form factor:

$$\begin{aligned}&\langle X(\lambda',P')|J^\mu_{\rm EM}|X(\lambda,P)\rangle \\ &= \left[F_{1X}(Q^2)\epsilon^*_{\lambda'}(P')\cdot\epsilon_\lambda(P) \right.\\ &\left. - F_{2X}(Q^2)\frac{q\cdot\epsilon_\lambda(P) q\cdot\epsilon^*_{\lambda'}(P')}{2m_X^2}\right](P+P')^\mu \\ &- F_{3X}(Q^2)[\epsilon^{\mu *}_{\lambda'}(P')q\cdot\epsilon_\lambda(P) - \epsilon^\mu_\lambda(P) q\cdot\epsilon^*_{\lambda'}(P')],\end{aligned} \tag{147}$$

with fixed momentum transfer $q = P' - P$ and $Q^2 = -q^2 = q_\perp^2$. They capture the charge and current distributions inside the hadron. For spin-1 mesons, we have three types of form factors: F_{1X}, F_{2X}, F_{X3}. From these form factors one can define the three Sachs form factors [78,79] for the spin-1 meson, namely, the charge $G_C^X(Q^2)$, the magnetic $G_M^X(Q^2)$, and the quadrupole $G_Q^X(Q^2)$ form factors. The relations between the Lorentz invariant form factors F_1^X, F_2^X, and F_3^X and the Sachs form factors are

$$G_C^X(Q^2) = F_{1X}(Q^2) + \frac{Q^2}{6m_X^2} G_Q^X(Q^2), \tag{148}$$

$$G_M^X(Q^2) = F_{3X}(Q^2), \tag{149}$$

$$G_Q^X(Q^2) = F_{1X}(Q^2) + \left(1 + \frac{Q^2}{4m_X^2}\right) F_{2X}(Q^2) - F_{3X}(Q^2). \tag{150}$$

In the presence of nonlocal interactions, the Noether construction is more subtle, as additional contributions from the emerging nonlocal interactions are needed to enforce current conservation in general [38,69,70]. Fortunately, in the light front formalism, the contributions from the nonlocal vertices of the emerging effective action do not contribute in the leading twist approximation [38]. Throughout, we will restrict our discussion of the EM form factors to the leading twist approximation.

The leading-twist form factor (charge form factor G_C^X) can be evaluated by the plus component of the spin-averaged meson matrix element in the $q^+ = 0$ frame,

(i) spin-0 meson form factor:

$$F_X(Q^2) = \frac{1}{2P^+}\langle X(P')|J^+_{\rm EM}|X(P)\rangle, \tag{151}$$

(ii) spin-1 meson form factor:

$$F_X(Q^2) = \frac{1}{2P^+}\left[\frac{1}{3}\sum_\lambda \langle X(\lambda,P')|J^+_{\rm EM}|X(\lambda,P)\rangle\right]. \tag{152}$$

If we choose a specific frame where $q^+ = 0$, with

$$P^\mu = \left(P^+, 0, \frac{m_X^2}{2P^+}\right), \qquad P'^\mu = \left(P^+, q_\perp, \frac{m_X^2 + q_\perp^2}{2P^+}\right),$$

the meson form factor follows as

$$F_X(Q^2)=\int_0^1 dx\int\frac{d^2k_\perp}{(2\pi)^3}\left[\Phi_X^*(x,k_\perp+\bar{x}q_\perp,s_1',s_2')Q_{f_1}\frac{\bar{u}_{s_1'}(k+q)\gamma^+u_{s_1}(k)}{2xP^+}\delta_{s_2',s_2}\Phi_X(x,k_\perp,s_1,s_2)\right.$$
$$\left.-\Phi_X^*(x,k_\perp-xq_\perp,s_1',s_2')Q_{f_2}\frac{\bar{v}_{s_2}(k)\gamma^+v_{s_2'}(k+q)}{2\bar{x}P^+}\delta_{s_1',s_1}\Phi_X(x,k_\perp,s_1,s_2)\right]. \tag{153}$$

More specifically, in the pion channel it is given by

$$F_\pi(Q^2)=\int_0^1 dx\int\frac{d^2k_\perp}{(2\pi)^3}\left[Q_u\phi_\pi(x,k_\perp+\bar{x}q_\perp)\phi_\pi(x,k_\perp)4\left(\frac{k_\perp^2+M^2+\bar{x}k_\perp\cdot q_\perp}{x\bar{x}}\right)\right.$$
$$\left.-Q_d\phi_\pi(x,k_\perp-xq_\perp)\phi_\pi(x,k_\perp)4\left(\frac{k_\perp^2+M^2-xk_\perp\cdot q_\perp}{x\bar{x}}\right)\right] \tag{154}$$

while in the vector channel it reads

$$F_{\omega,\rho}(Q^2)=\int_0^1 dx\int\frac{d^2k_\perp}{(2\pi)^3}\left[Q_u\phi_{\omega,\rho}(x,k_\perp+\bar{x}q_\perp)\phi_{\omega,\rho}(x,k_\perp)\frac{8}{3}\left(\frac{k_\perp^2+(1+2x\bar{x})M^2+\bar{x}k_\perp\cdot q_\perp}{x\bar{x}}\right)\right.$$
$$\left.-Q_d\phi_{\omega,\rho}(x,k_\perp-xq_\perp)\phi_{\omega,\rho}(x,k_\perp)\frac{8}{3}\left(\frac{k_\perp^2+(1+2x\bar{x})M^2-xk_\perp\cdot q_\perp}{x\bar{x}}\right)\right]. \tag{155}$$

To proceed, it is useful to parametrize the nonlocal form factor using

$$z_\pm=\left[z^2\pm\frac{\bar{x}\rho q_\perp}{2\lambda_X\sqrt{x\bar{x}}}z\cos\theta+\frac{\bar{x}^2\rho^2q_\perp^2}{16x\bar{x}\lambda_X^2}\right]^{1/2}$$

so that

$$\mathcal{F}_M(z,x,\theta)=(z_+F'(z_+))^2(z_-F'(z_-))^2.$$

With this in mind, the pion form factor can be worked out:

$$F_\pi(Q^2)=\frac{C_\pi^2}{2\pi^2}\int_0^{2\pi}\frac{d\theta}{2\pi}\int_0^1 dx\int_0^\infty dz x\bar{x}z\left(\frac{2}{3}\frac{x\bar{x}z^2+\frac{\rho^2M^2}{4\lambda_S^2}-\frac{\bar{x}^2\rho^2q_\perp^2}{16\lambda_S^2}}{\left[\left(x\bar{x}z^2-\frac{\rho^2}{4\lambda_S^2}(x\bar{x}m_\pi^2-M^2)+\frac{\bar{x}^2\rho^2q_\perp^2}{16\lambda_S^2}\right)^2-\frac{\bar{x}^2\rho^2q_\perp^2}{4\lambda_S^2}x\bar{x}z^2\cos^2\theta\right]}\mathcal{F}_M(z,x,\theta)\right.$$
$$\left.+\frac{1}{3}\frac{x\bar{x}z^2+\frac{\rho^2M^2}{4\lambda_S^2}-\frac{x^2\rho^2q_\perp^2}{16\lambda_S^2}}{\left[\left(x\bar{x}z^2-\frac{\rho^2}{4\lambda_S^2}(x\bar{x}m_\pi^2-M^2)+\frac{x^2\rho^2q_\perp^2}{16\lambda_S^2}\right)^2-\frac{x^2\rho^2q_\perp^2}{4\lambda_S^2}x\bar{x}z^2\cos^2\theta\right]}\mathcal{F}_M(z,\bar{x},\theta)\right). \tag{156}$$

The pion EM form factor in (156) accounts for only the coupling to the lowest Fock component of the pion on the light front. While it accounts properly for the charge normalization, it falls short from accounting for the rho-meson cloud at nonvanishing Q^2, which is a coherent multi-Fock component. For small Q^2, the pion sources a rho meson, which is readily obtained by resumming the bubble chain in the t channel in our light front formulation, in line with vector meson dominance (VMD) [80] (and references therein),

$$F_\pi^{\rm VDM}(Q^2)=F_\pi(0)\frac{1}{1+Q^2/m_{\omega,\rho}^2}. \tag{157}$$

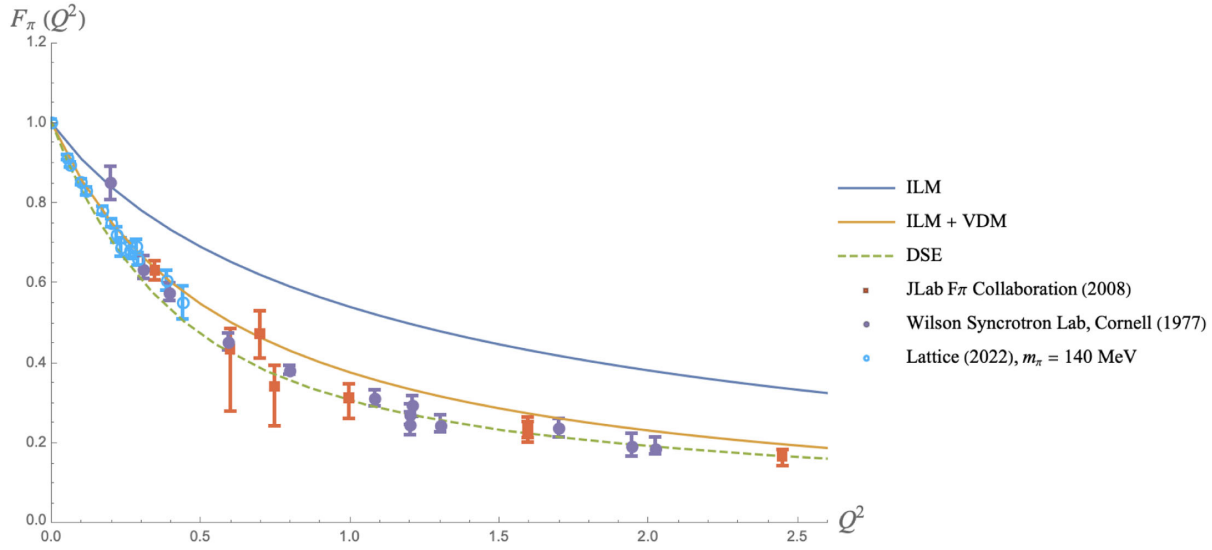

FIG. 22. Our results in solid blue (undressed) and solid orange (dressed) for the pion EM form factor are compared with the JLab measurements in red squares [81] and the Cornell measurements in purple dots [82,83]. The recent lattice calculations are shown in blue triangles [84], and the Dyson-Schwinger results are shown in dashed green [85].

The EM form factors of the vector mesons follow similarly:

$$F_{\omega,\rho}(Q^2)=\frac{C^2_{\omega,\rho}}{3\pi^2}\int_0^{2\pi}\frac{d\theta}{2\pi}\int_0^1 dx\int_0^\infty dz x\bar{x}z\left(\frac{2}{3}\frac{x\bar{x}z^2+\frac{\rho^2M^2}{4\lambda_V^2}(1+2x\bar{x})-\frac{\bar{x}^2\rho^2q_\perp^2}{16\lambda_V^2}}{\left[\left(x\bar{x}z^2-\frac{\rho^2}{4\lambda_V^2}(x\bar{x}m^2_{\omega,\rho}-M^2)+\frac{\bar{x}^2\rho^2q_\perp^2}{16\lambda_V^2}\right)^2-\frac{\bar{x}^2\rho^2q_\perp^2}{4\lambda_V^2}x\bar{x}z^2\cos^2\theta\right]}\mathcal{F}_M(z,x,\theta)\right.$$
$$\left.+\frac{1}{3}\frac{x\bar{x}z^2+\frac{\rho^2M^2}{4\lambda_V^2}(1+2x\bar{x})-\frac{x^2\rho^2q_\perp^2}{16\lambda_V^2}}{\left[\left(x\bar{x}z^2-\frac{\rho^2}{4\lambda_V^2}(x\bar{x}m^2_{\omega,\rho}-M^2)+\frac{x^2\rho^2q_\perp^2}{16\lambda_V^2}\right)^2-\frac{x^2\rho^2q_\perp^2}{4\lambda_V^2}x\bar{x}z^2\cos^2\theta\right]}\mathcal{F}_M(z,\bar{x},\theta)\right). \tag{158}$$

In Fig. 22 we show the bare pion form factor (156) in solid blue and the rho-meson dressed pion form factor (157) in solid orange, versus Q^2. Our results in the QCD instanton vacuum are compared to the measurement using pion scattering from the reaction ${}^1H(e,e'\pi^+)n$ by the JLab F_π Collaboration in red squares [81], the Cornell Collaboration in purple dots [82,83], and the lattice results in blue triangles [84]. The Dyson-Schwinger results with rainbow ladders are shown in dashed green [85]. Clearly, our lowest undressed Fock contribution fails to reproduce the pion EM form factor, while the dressed multi-Fock component agrees relatively well with the current measurements. This result underlies the collective character of the pion state.

In Fig. 23 we show the EM form factor of the rho meson in blue solid versus Q^2, in comparison to the lattice data in green squares from the Hadron Spectrum Collaboration [86]. The results from the Bethe-Salpeter in the NJL model are shown in dashed orange. The falloff of the form factor is sharper in our case in comparison to the lattice results, reflecting on a larger charge radius for the rho. This falloff is sensitive to the value of λ_V in (79) fixed by the rho weak decay constants. A larger value of λ_V yields a smaller charge radius, at the expense of the weak decay constants. We note that the falloff of our rho form factor is slower than that reported in [51,87–89], but about similar to the reported lattice results. In Fig. 24, we compare the EM form factors for the pion undressed in dashed blue, dressed in solid orange, with the EM form factor of the vector mesons in solid green.

On the light front, all hadrons are 2D Lorentz contracted. The light front radius r_X follows from

$$F_X(Q^2)=1-\frac{Q^2}{6}r_X^2+\mathcal{O}(Q^4). \tag{159}$$

For the pion EM form factor, we have

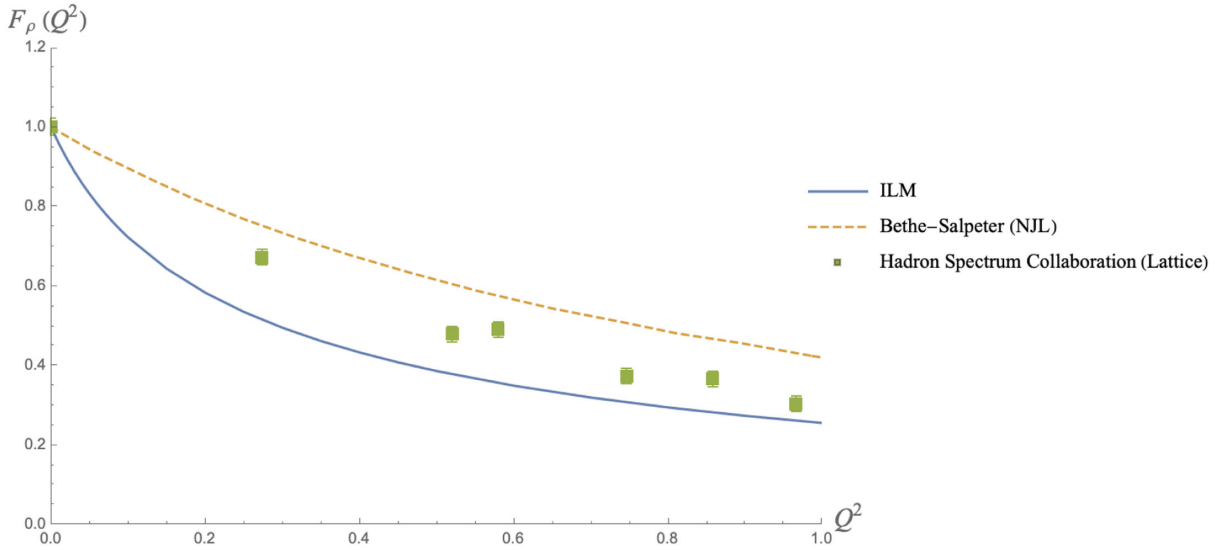

FIG. 23. Our calculations are compared with the recent lattice calculation [86] and the model analysis by Bethe-Salpeter equation using the random-phase approximation in the NJL model [78].

$$r_\pi = 0.489 \text{ fm},$$
$$r_\pi^{\text{VDM}} = 0.620 \text{ fm},$$
$$r_\pi^{\text{exp}} = 0.659 \pm 0.004 \text{ fm}. \quad (160)$$

The charge radius from other work can also be found in

Reference	r_π (fm)
ILM (this work)	0.620
Faessler [41]	0.650
Hutauruk [40]	0.629

Without the rho cloud, the bare EM size of the pion r_π is slightly larger than the size of an instanton $\rho = 0.313$ fm. Pions are collective Goldstone modes, strongly bound by single instantons (anti-instantons) of size ρ. In contrast, the EM size of the rho and omega $r_{\omega,\rho} = 0.997$ fm is about twice the pion size. Vector mesons are bound by molecular configurations of size about 2ρ. As we noted, the empirical value of the charge radius for the pion r_π^{exp} in [61,90] compares well only with the dressed pion, in line with the VMD lore. For completeness, we compare our charge radius for the rho meson with some model calculations in the table.

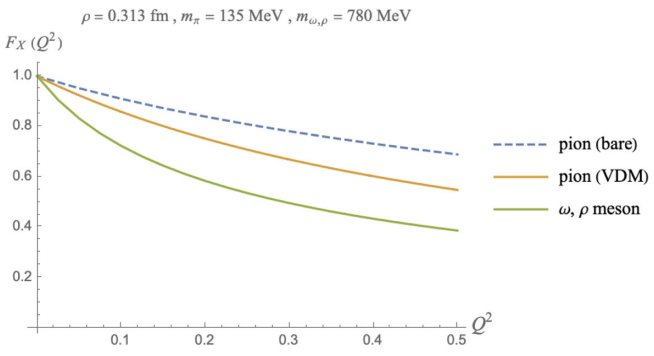

FIG. 24. Pion EM form factor in dashed blue (undressed) and in solid orange (dressed) in comparison to the vector EM form factor in solid green.

Reference	r_ρ (fm)
ILM (this work)	0.997
de Melo [87]	0.608
Bhagwat [91]	0.735
Krutov [92]	0.748
Carrillo-Serrano [78]	0.819
Owen [93]	0.819

IX. CONCLUSIONS

We presented a detailed analysis of the emerging 't Hooft nonlocal interactions on the light front, in the light scalar and pseudoscalar channels. These interactions include not only the standard single instanton and anti-instanton chirality flipping contributions, but also the molecular chirality preserving contributions. The diluteness of the instanton tunneling rates in the QCD vacuum makes the molecular contributions parametrically small. Their contribution is subleading in the spontaneous breaking of chiral symmetry, yet leading in the formation of the light vector mesons.

Our analysis focused on the light front formulation, where the light quark fields are split into a good plus bad component. The elimination of the bad component

generates additional multifermion interactions. Using the $1/N_c$ bookkeeping analysis, we have shown that in leading order these additional interactions are tadpolelike and can be resummed to renormalize the nonlocal interactions between the good components. They are at the origin of the nontrivial vacuum structure on the light front, as initially observed in the NJL model with local interactions [56–58]. Contrary to common lore, the vacuum is nontrivial on the light front.

The light front Hamiltonian associated to the emerging nonlocal effective action was used to define the eigenvalue problem for the light scalar and vector meson states, limited to their lowest Fock component. The explicit breaking of Lorentz symmetry yields apparently different equations for the longitudinally and transversely polarized rho and omega vector mesons. Fortunately, a thorough analysis of the longitudinal equation shows that the difference is amenable to the ratio of the vector to scalar interaction strengths, which is parametrically small in the QCD instanton vacuum.

Our light front results for the light scalar and vector mesons PDFs and DAs are evaluated at a low renormalization point of about $1/2\rho \sim 0.31$ GeV. A comparison to existing measurements and lattice simulations at a scale of $\mu = 2$ GeV requires evolution. For simplicity, we have assumed that factorization holds at this relatively low scale, and used perturbative QCD evolution. Our results were shown to be remarkably consistent with most measurements. Yet a more appropriate evolution from this low renormalization scale should perhaps make use of nonperturbative effects [16]. This will be discussed elsewhere.

Finally, we have used the light front wave functions in the QCD instanton vacuum to analyze the EM form factors of the pions and rho and omega vector mesons. The leading Fock state in the rho meson yields a rho EM form factor in good agreement with the recently reported lattice simulations. This is not the case of the pion, when limited to its lowest Fock component, a well-known shortcoming. This is readily fixed by resumming the leading rho contribution to the pion EM form factor, in line with the tenets of vector dominance.

ACKNOWLEDGMENTS

This work is supported by the Office of Science, U.S. Department of Energy under Contract No. DE-FG-88ER40388.

APPENDIX A: LORENTZ COVARIANT FORMALISM: BETHE-SALPETER EQUATION

To investigate the meson structures in a covariant frame, we can organize the Bethe-Salpeter kernel in $1/N_c$. In leading order (LO), the vacuum polarization function contributes to the 4-point function through the bubble chain

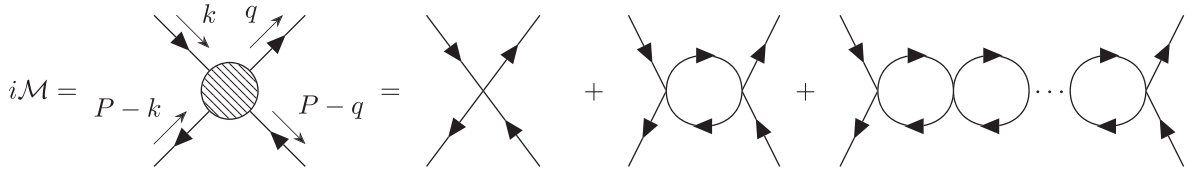

The next-to-leading order (NLO) is more involved [94]. Using our emerging action for the light quarks with nonlocal interactions, the vacuum polarization function $\Pi^{\alpha\beta}$ is given by

$$\Pi^{\alpha\beta} = -i\int \frac{d^4k}{(2\pi)^4} \frac{\mathrm{tr}[\Gamma^\alpha(\not{k} + M(k))\Gamma^\beta(\not{P} - \not{k} - M(P-k))]}{[k^2 - M^2(k)][(P-k)^2 - M^2(P-k)]} \mathcal{F}(k)\mathcal{F}(P-k) \tag{A1}$$

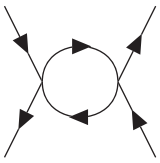

where $\Gamma^\alpha = 1, i\gamma^5, \tau^a, i\gamma^5\tau^a, \gamma^\mu, \gamma^\mu\tau^a, \gamma^\mu\gamma^5, \gamma^\mu\gamma^5\tau^a$ for $\sigma, \eta', a_0, \pi, \omega, \rho, f_1, a_1$ respectively. In the low momentum limit ($k \ll 1/\rho$), similar to the approximation we imposed in the gap equation. We approximate the momentum-dependent constituent mass $M(k)$ in the fermionic bubble functions by $M(0)$, and the emergent constituent mass at zero momentum,

$$\int \frac{d^4k}{(2\pi)^4} \Pi_X(M(k), M(P-k)) \approx \int \frac{d^4k}{(2\pi)^4} \Pi_X(M, M).$$

The vacuum polarization function Π in the low momentum limit simplifies

$$\Pi_X^{\alpha\beta} = -i \int \frac{d^4k}{(2\pi)^4} \frac{\mathrm{tr}[\Gamma^\alpha(\not{k}+M)\Gamma^\beta(\not{P}-\not{k}-M)]}{(k^2-M^2)((P-k)^2-M^2)} \mathcal{F}(k)\mathcal{F}(P-k). \tag{A2}$$

1. Scalar channel

In the scalar channel and close to the pole, the resummation of the vacuum polarizations gives

$$i\mathcal{M} = \bar{u}_{s_1'}(q) v_{s_2'}(P-q) \sqrt{\mathcal{F}(q)\mathcal{F}(P-q)} D_\sigma(P^2) \sqrt{\mathcal{F}(k)\mathcal{F}(P-k)} \bar{v}_{s_2}(P-k) u_{s_1}(k), \tag{A3}$$

$$i\mathcal{M} = \bar{u}_{s_1'}(q) \tau^a v_{s_2'}(P-q) \sqrt{\mathcal{F}(q)\mathcal{F}(P-q)} D_{a_0}(P^2) \sqrt{\mathcal{F}(k)\mathcal{F}(P-k)} \bar{v}_{s_2}(P-k) \tau^a u_{s_1}(k), \tag{A4}$$

with the scalar propagator

$$D_{\sigma,a_0}(P^2) = \frac{iG_{\sigma,a_0}}{1 - G_{\sigma,a_0}\Pi_{SS}(P^2)}. \tag{A5}$$

The scalar vacuum polarization function is

$$\begin{aligned}\Pi_{SS} &= -2iN_c \int \frac{d^4k}{(2\pi)^4} \frac{\mathrm{tr}[(\not{k}+M)(\not{P}-\not{k}-M)]}{(k^2-M^2)((P-k)^2-M^2)} \mathcal{F}(k)\mathcal{F}(P-k) \\ &= -2iN_c \int \frac{d^4k}{(2\pi)^4} \frac{4k\cdot(P-k)-4M^2}{(k^2-M^2)((P-k)^2-M^2)} \mathcal{F}(k)\mathcal{F}(P-k).\end{aligned} \tag{A6}$$

2. Pseudoscalar channel

In the pseudoscalar channel, the resummation gives

$$i\mathcal{M} = \bar{u}_{s_1'}(q) i\gamma^5 v_{s_2'}(P-q) \sqrt{\mathcal{F}(q)\mathcal{F}(P-q)} D_{\eta'}(P^2) \sqrt{\mathcal{F}(k)\mathcal{F}(P-k)} \bar{v}_{s_2}(P-k) i\gamma^5 u_{s_1}(k), \tag{A7}$$

$$i\mathcal{M} = \bar{u}_{s_1'}(q) i\gamma^5 \tau^a v_{s_2'}(P-q) \sqrt{\mathcal{F}(q)\mathcal{F}(P-q)} D_\pi(P^2) \sqrt{\mathcal{F}(k)\mathcal{F}(P-k)} \bar{v}_{s_2}(P-k) i\gamma^5 \tau^a u_{s_1}(k), \tag{A8}$$

with the pseudoscalar propagator

$$D_{\pi,\eta'}(P^2) = \frac{iG_{\pi,\eta'}}{1 - G_{\pi,\eta'}\Pi_{PP}(P^2)}. \tag{A9}$$

The pseudoscalar vacuum polarization is

$$\begin{aligned}\Pi_{PP} &= -2iN_c \int \frac{d^4k}{(2\pi)^4} \frac{\mathrm{tr}[(\not{k}+M) i\gamma^5 (\not{P}-\not{k}-M) i\gamma^5]}{(k^2-M^2)((P-k)^2-M^2)} \mathcal{F}(k)\mathcal{F}(P-k) \\ &= -2iN_c \int \frac{d^4k}{(2\pi)^4} \frac{4k\cdot(P-k)+4M^2}{(k^2-M^2)((P-k)^2-M^2)} \mathcal{F}(k)\mathcal{F}(P-k).\end{aligned} \tag{A10}$$

We have neglected the pseudoscalar-axial mixing as higher order in g_V/g_S.

3. Vector channel

In the vector channel, the vacuum polarization function can be rearranged through

$$\Pi^{\mu\nu}_{VV} = -2iN_c \int \frac{d^4k}{(2\pi)^4} \frac{\mathrm{tr}[(\not{k}+M)\gamma^\mu(\not{P}-\not{k}-M)\gamma^\nu]}{(k^2-M^2)((P-k)^2-M^2)} \mathcal{F}(k)\mathcal{F}(P-k)$$
$$= -\Pi_{VV}(P^2)\left(g^{\mu\nu} - \frac{P^\mu P^\nu}{P^2}\right) \tag{A11}$$

with manifest current conservation $P_\mu \Pi^{\mu\nu}_{\omega,\rho} = 0$. The resummation of the fermionic chains gives

$$i\mathcal{M} = \bar{u}_{s_1'}(q)\gamma_\mu v_{s_2'}(P-q)\sqrt{\mathcal{F}(q)\mathcal{F}(P-q)} D^{\mu\nu}_\omega(P^2)\sqrt{\mathcal{F}(k)\mathcal{F}(P-k)}\bar{v}_{s_2}(P-k)\gamma_\nu u_{s_1}(k), \tag{A12}$$

$$i\mathcal{M} = \bar{u}_{s_1'}(q)\gamma_\mu \tau^a v_{s_2'}(P-q)\sqrt{\mathcal{F}(q)\mathcal{F}(P-q)} D^{\mu\nu}_\rho(P^2)\sqrt{\mathcal{F}(k)\mathcal{F}(P-k)}\bar{v}_{s_2}(P-k)\gamma_\nu \tau^a u_{s_1}(k), \tag{A13}$$

with the vector propagator

$$D^{\mu\nu}_{\omega,\rho}(P^2) = \frac{-iG_{\omega,\rho}}{1 - G_{\omega,\rho}\Pi_{\omega,\rho}(P^2)}\left(g^{\mu\nu} - G_{\omega,\rho}\Pi_{VV}(P^2)\frac{P^\mu P^\nu}{P^2}\right) \tag{A14}$$

where

$$\Pi_{VV} = -2iN_c \frac{4}{3}\int \frac{d^4k}{(2\pi)^4} \frac{2k\cdot(P-k)+4M^2}{(k^2-M^2)((P-k)^2-M^2)} \mathcal{F}(k)\mathcal{F}(P-k). \tag{A15}$$

The scattering amplitude develops poles at the location of the bound states, whenever

$$G_X \Pi_X(m_X^2) = 1 \tag{A16}$$

with $P^2 = m_X^2$. This fixes the mass eigenvalue equation. If we only consider the 't Hooft Lagrangian, the single instanton and anti-instanto interactions for σ and π are attractive, while those for η' and a_0 are repulsive. The molecular interactions ω, ρ, and a_1 are attractive within a certain range, but repulsive in the f_1 channel.

APPENDIX B: BOUND STATE EQUATION OF LONGITUDINAL VECTOR MESON

The bound state equation for the longitudinal meson on the light front is not only more involved than that of its transverse counterpart, but apparently different. Here, we detail its derivation, and show that the differences can be removed thanks to a number of identities. More specifically, the longitudinally bound state equation can be readily cast in the form

$$m^2_{\omega,\rho}\left(1+\frac{k_\perp^2+M^2}{m^2_{\omega,\rho}x\bar{x}}\right)\phi_{\omega,\rho}(x,k_\perp) = \frac{k_\perp^2+M^2}{x\bar{x}}\left(1+\frac{k_\perp^2+M^2}{m^2_{\omega,\rho}x\bar{x}}\right)\phi_{\omega,\rho}(x,k_\perp) - \frac{8g_{\omega,\rho}}{\sqrt{2x\bar{x}}}\sqrt{\mathcal{F}(k)\mathcal{F}(P-k)}\int \frac{dyd^2q_\perp}{\sqrt{2y\bar{y}}(2\pi)^3}$$
$$\times\left[\frac{q_\perp^2+M^2}{y\bar{y}} - 4g_{\omega,\rho}w_-(P^+)(P^+)^2\right]\left(y\bar{y}+\frac{q_\perp^2+M^2}{m^2_{\omega,\rho}}\right)\phi_{\omega,\rho}(y,q_\perp)\sqrt{\mathcal{F}(q)\mathcal{F}(P-q)}$$
$$-\frac{8g_{\omega,\rho}}{\sqrt{2x\bar{x}}}\sqrt{\mathcal{F}(k)\mathcal{F}(P-k)}\left[\frac{k_\perp^2+M^2}{x\bar{x}} - 4g_{\omega,\rho}w_-(P^+)(P^+)^2\right]$$
$$\times\int\frac{dyd^2q_\perp}{\sqrt{2y\bar{y}}(2\pi)^3}\left(y\bar{y}+\frac{q_\perp^2+M^2}{m^2_{\omega,\rho}}\right)\phi_{\omega,\rho}(y,q_\perp)\sqrt{\mathcal{F}(q)\mathcal{F}(P-q)}. \tag{B1}$$

The tadpole resummation involved in the bound state equation of the longitudinal mode can be rearranged as

$$
\begin{aligned}
w_-(P^+) &= \int \frac{dk^+ d^2k_\perp}{(2\pi)^3} \frac{(k_\perp^2+M^2)\epsilon(k^+)}{2(k^+)^2(P^+-k^+)} \mathcal{F}(k)\mathcal{F}(P-k) \\
&= \frac{1}{(P^+)^2} \int \frac{dx d^2k_\perp}{(2\pi)^3} \frac{(k_\perp^2+M^2)\epsilon(x)}{2x^2\bar{x}} \mathcal{F}(k)\mathcal{F}(P-k) \\
&= \frac{1}{(P^+)^2} \int_0^1 dx \int \frac{d^2k_\perp}{(2\pi)^3} \frac{(k_\perp^2+M^2)}{2x\bar{x}} \mathcal{F}(k)\mathcal{F}(P-k) \\
&= \eta \frac{m_{\omega,\rho}^2}{2(P^+)^2}.
\end{aligned} \tag{B2}
$$

Remarkably the complicated result (B1) can be considerably simplified by noting that it is composed of three integrals

$$
\begin{aligned}
H_1 &= \int \frac{dy}{\sqrt{2y\bar{y}}} \int \frac{d^2q_\perp}{(2\pi)^3} (y\bar{y}m_{\omega,\rho}^2 + q_\perp^2 + M^2)\phi_{\omega,\rho}(y,q_\perp)\sqrt{\mathcal{F}(q)\mathcal{F}(P-q)}, \\
H_2 &= \int \frac{dy}{\sqrt{2y\bar{y}}} \int \frac{d^2q_\perp}{(2\pi)^3} (y\bar{y}m_{\omega,\rho}^2 + q_\perp^2 + M^2)\left(\frac{q_\perp^2+M^2}{y\bar{y}m_{\omega,\rho}^2}\right)\phi_{\omega,\rho}(y,q_\perp)\sqrt{\mathcal{F}(q)\mathcal{F}(P-q)} \\
\eta &= \int \frac{dy d^2q_\perp}{(2\pi)^3} \frac{q_\perp^2+M^2}{m_{\omega,\rho}^2 y\bar{y}} \mathcal{F}(q)\mathcal{F}(P-q).
\end{aligned}
$$

The integrals H_1 and H_2 are not independent of each other. Indeed, if we multiply (B1) by $\sqrt{2x\bar{x}}$ and $\sqrt{\mathcal{F}(q)\mathcal{F}(P-q)}$, and integrate the result over the momentum phase space, we have

$$
H_2 = \frac{H_1}{1 - 4g_{\omega,\rho}\int \frac{dyd^2q_\perp}{(2\pi)^3}\mathcal{F}(q)\mathcal{F}(P-q)} + 4g_{\omega,\rho}\eta H_1. \tag{B3}
$$

Inserting (B3) in (B1), the equation simplifies to

$$
\begin{aligned}
\left(m_{\omega,\rho}^2 - \frac{k_\perp^2+M^2}{x\bar{x}}\right)\phi_{\omega,\rho}(x,k_\perp) &= -8g_{\omega,\rho}\left[1 - 4g_{\omega,\rho}\int \frac{dyd^2q_\perp}{(2\pi)^3}\mathcal{F}(q)\mathcal{F}(P-q)\right]^{-1}\left[1 - 4g_{\omega,\rho}\left(\int \frac{dyd^2q_\perp}{(2\pi)^3}\mathcal{F}(q)\mathcal{F}(P-q)\right)\right. \\
&\quad \left.\times \left(\frac{k_\perp^2+M^2}{m_{\omega,\rho}^2 x\bar{x} + k_\perp^2 + M^2}\right)\right]\frac{1}{\sqrt{2x\bar{x}}}\sqrt{\mathcal{F}(k)\mathcal{F}(P-k)}\int \frac{dy}{\sqrt{2y\bar{y}}} \\
&\quad \times \int \frac{d^2q_\perp}{(2\pi)^3}(y\bar{y}m_{\omega,\rho}^2 + q_\perp^2 + M^2)\phi_{\omega,\rho}(y,q_\perp)\sqrt{\mathcal{F}(q)\mathcal{F}(P-q)} \\
&\simeq -\frac{8g_{\omega,\rho}}{\sqrt{2x\bar{x}}}\frac{\sqrt{\mathcal{F}(k)\mathcal{F}(P-k)}}{1 - 4g_{\omega,\rho}\int \frac{dyd^2q_\perp}{(2\pi)^3}\mathcal{F}(q)\mathcal{F}(P-q)}\int \frac{dy}{\sqrt{2y\bar{y}}} \\
&\quad \times \int \frac{d^2q_\perp}{(2\pi)^3}(y\bar{y}m_{\omega,\rho}^2 + q_\perp^2 + M^2)\phi_{\omega,\rho}(y,q_\perp)\sqrt{\mathcal{F}(q)\mathcal{F}(P-q)}
\end{aligned} \tag{B4}
$$

where we dropped the higher order terms in $\mathcal{O}(g_{\omega,\rho}^2)$ in the third equality. As we argued in the main text, the QCD instanton vacuum is dilute, with the contributions $g_{\omega,\rho}/g_S$ parametrically small. We have only kept them in leading order in the vector channels, as their keeping at next-to-leading order involves a more complex bookkeeping procedure. With this in mind, we can further simplify (B4) by multiplying it by $\sqrt{2x\bar{x}}$ and $\sqrt{\mathcal{F}(q)\mathcal{F}(P-q)}$ again, and integrating over x and $k_\perp$. The result is

$$
\begin{aligned}
&\int \frac{dxd^2k_\perp}{(2\pi)^3}\sqrt{2x\bar{x}}\sqrt{\mathcal{F}(k)\mathcal{F}(P-k)}\left(m_{\omega,\rho}^2 - \frac{k_\perp^2+M^2}{x\bar{x}}\right)\phi_{\omega,\rho}(x,k_\perp) \\
&= -8g_{\omega,\rho}\int \frac{dyd^2q_\perp}{(2\pi)^3}\mathcal{F}(q)\mathcal{F}(P-q)\int \frac{dxd^2k_\perp}{(2\pi)^3}\sqrt{2x\bar{x}}\sqrt{\mathcal{F}(k)\mathcal{F}(P-k)}\left(\frac{k_\perp^2+M^2}{x\bar{x}}\right)\phi_{\omega,\rho}(x,k_\perp)
\end{aligned} \tag{B5}
$$

hence the bound state equation

$$\left(m_{\omega,\rho}^2-\frac{k_\perp^2+M^2}{x\bar{x}}\right)\phi_{\omega,\rho}(x,k_\perp)\simeq-\frac{16g_{\omega,\rho}}{\sqrt{2x\bar{x}}}\sqrt{\mathcal{F}(k)\mathcal{F}(P-k)}\int\frac{dy}{\sqrt{2y\bar{y}}}\int\frac{d^2q_\perp}{(2\pi)^3}(q_\perp^2+M^2)\phi_{\omega,\rho}(y,q_\perp)\sqrt{\mathcal{F}(q)\mathcal{F}(P-q)}. \tag{B6}$$

APPENDIX C: LIGHT FRONT WAVE FUNCTIONS WITH $P_\perp \neq 0$

To obtain the off-diagonal hadronic matrix elements, we need to generalize the light front wave functions to a frame with $P_\perp \neq 0$. In this frame, the hadronic momentum is

$$P^\mu=\left(P^+,P_\perp,\frac{P_\perp^2+m_X^2}{2P^+}\right).$$

The quark k_1 and antiquark k_2 momenta can be parametrized by

$$k_1^\mu=\left(xP^+,xP_\perp+k_\perp,\frac{(xP_\perp+k_\perp)^2+M^2}{2xP^+}\right),$$

$$k_2^\mu=\left(\bar{x}P^+,\bar{x}P_\perp-k_\perp,\frac{(\bar{x}P_\perp-k_\perp)^2+M^2}{2\bar{x}P^+}\right).$$

For the spin-1 meson, the polarization vector $\epsilon_\lambda^\mu(P)$ is defined as

$$\epsilon_\pm^\mu(P)=\frac{1}{\sqrt{2}}\left(0,1,\pm i,\frac{P^1\pm iP^2}{P^+}\right),$$

$$\epsilon_0^\mu(P)=\frac{1}{m_X}\left(P^+,\frac{P^1}{2},\frac{P^2}{2},\frac{P_\perp^2-m_X^2}{2P^+}\right).$$

With this symmetric parametrization, the light front wave functions have the same form. The spin-independent wave functions are

$$\phi_X(x,k_\perp)=\frac{C_X}{\sqrt{2x\bar{x}}(m_X^2-\frac{k_\perp^2+M^2}{x\bar{x}})}\sqrt{\mathcal{F}(k)\mathcal{F}(P-k)}; \tag{C1}$$

scalar channels:

$$\Phi_\sigma(x,k_\perp,s_1,s_2)=\frac{1}{\sqrt{N_c}}\phi_\sigma(x,k_\perp)\bar{u}_{s_1}(k)v_{s_2}(P-k), \tag{C2}$$

$$\Phi_{a_0}(x,k_\perp,s_1,s_2)=\frac{1}{\sqrt{N_c}}\phi_{a_0}(x,k_\perp)\bar{u}_{s_1}(k)\tau^a v_{s_2}(P-k); \tag{C3}$$

pseudoscalar channels:

$$\Phi_{\eta'}(x,k_\perp,s_1,s_2)=\frac{1}{\sqrt{N_c}}\phi_{\eta'}(x,k_\perp)\bar{u}_{s_1}(k)i\gamma^5 v_{s_2}(P-k), \tag{C4}$$

$$\Phi_\pi(x,k_\perp,s_1,s_2)=\frac{1}{\sqrt{N_c}}\phi_\pi(x,k_\perp)\bar{u}_{s_1}(k)i\gamma^5\tau^a v_{s_2}(P-k); \tag{C5}$$

vector channels:

$$\Phi_\omega^\lambda(x,k_\perp,s_1,s_2)=\frac{1}{\sqrt{N_c}}\phi_\omega(x,k_\perp)\epsilon_\lambda^\mu(P)\bar{u}_{s_1}(k)\gamma_\mu v_{s_2}(P-k), \tag{C6}$$

$$\Phi_\rho^\lambda(x,k_\perp,s_1,s_2)=\frac{1}{\sqrt{N_c}}\phi_\rho(x,k_\perp)\epsilon_\lambda^\mu(P)\bar{u}_{s_1}(k)\gamma_\mu\tau^a v_{s_2}(P-k). \tag{C7}$$

APPENDIX D: SPIN-DEPENDENT WAVE FUNCTIONS ON THE LIGHT FRONT

The spin-dependent wave functions denote the spin states in the creation of a quark-antiquark pair. The wave functions for each channels are as follows:

scalar:

$$\bar{u}_{s_1}(k)v_{s_2}(P-k)=\frac{1}{\sqrt{x\bar{x}}}\chi_{s_1}^\dagger[M(\bar{x}-x)\sigma_z-k_\perp\cdot\sigma_\perp]\eta_{s_2}; \tag{D1}$$

pseudoscalar:

$$\bar{u}_{s_1}(k)i\gamma^5 v_{s_2}(P-k)=\frac{i}{\sqrt{x\bar{x}}}\chi_{s_1}^\dagger[M-k_\perp\cdot\sigma_\perp\sigma_z]\eta_{s_2}; \tag{D2}$$

vector:

$$\epsilon_+^\mu(P)\bar{u}_{s_1}(k)\gamma_\mu v_{s_2}(P-k) = -\frac{1}{\sqrt{x\bar{x}}}\chi_{s_1}^\dagger\left[\sqrt{2}M\sigma^+ + \left(\bar{x}\frac{1+\sigma_z}{\sqrt{2}} + x\frac{1-\sigma_z}{\sqrt{2}}\right)k_R\right]\eta_{s_2}, \tag{D3}$$

$$\epsilon_-^\mu(P)\bar{u}_{s_1}(k)\gamma_\mu v_{s_2}(P-k) = -\frac{1}{\sqrt{x\bar{x}}}\chi_{s_1}^\dagger\left[\sqrt{2}M\sigma^- - \left(\bar{x}\frac{1-\sigma_z}{\sqrt{2}} + x\frac{1+\sigma_z}{\sqrt{2}}\right)k_L\right]\eta_{s_2}, \tag{D4}$$

$$\epsilon_0^\mu(P)\bar{u}_{s_1}(k)\gamma_\mu v_{s_2}(P-k) = -\frac{m_X}{2P^+}\left(1+\frac{k_\perp^2+M^2}{x\bar{x}m_X^2}\right)\frac{1}{\sqrt{x\bar{x}}}\chi_{s_1}^\dagger 2x\bar{x}P^+\sigma_z\eta_{s_2}, \tag{D5}$$

where $\sigma^\pm = (\sigma_x \pm i\sigma_y)/2$ and $k_{L,R} = k^1 \pm ik^2$.

APPENDIX E: ERBL EVOLUTION

At the leading twist, we have three types of distribution amplitudes defined by vector, axial vector, and tensor currents. In this work, the pion axial DA, vector DA of ω and ρ, and their tensor DAs are discussed. Without loss of generality, we only display the isovector states for the ERBL evolution:

$$\langle 0|\bar{\psi}(0)\gamma^+\gamma^5\frac{\tau^a}{\sqrt{2}}W(0,\xi^-)\psi(\xi^-)|\pi(P)\rangle = if_\pi P^+\int_0^1 dx e^{-ixP^+\xi^-}\phi_\pi^A(x), \tag{E1}$$

$$\langle 0|\bar{\psi}(0)\gamma^+\frac{\tau^a}{\sqrt{2}}W(0,\xi^-)\psi(\xi^-)|\rho(\lambda,P)\rangle = f_\rho m_\rho\epsilon_\lambda^+(P)\int_0^1 dx e^{-ixP^+\xi^-}\phi_\rho^V(x), \tag{E2}$$

$$\langle 0|\bar{\psi}(0)i\gamma^+\gamma_\perp^i\frac{\tau^a}{\sqrt{2}}W(0,\xi^-)\psi(\xi^-)|\rho(\lambda,P)\rangle = -if_\rho^T P^+\epsilon_\lambda^i(P)\int_0^1 dx e^{-ixP^+\xi^-}\phi_\rho^T(x). \tag{E3}$$

The DAs can be expanded in terms of Gegenbauer polynomials $C_n^{3/2}(x-\bar{x})$. This expansion is around the asymptotic form $6x(1-x) = 6x\bar{x}$ predicted by perturbative QCD in the Bjorken limit,

$$\phi^{A,V,T}(x,\mu) = 6x\bar{x}\sum_{n=0}^{\infty}C_n^{3/2}(x-\bar{x})a_n^{A,V,T}(\mu). \tag{E4}$$

Due to the orthogonality of the Gegenbauer polynomials, the coefficient can be obtained by

$$a_n^{A,V,T}(\mu) = \frac{2(2n+3)}{3(n+1)(n+2)}\int_0^1 dy C_n^{3/2}(y-\bar{y})\phi^{A,V,T}(y,\mu). \tag{E5}$$

Using the Gegenbauer polynomial basis $C_n^m(z)$, we can convert the integrodifferential equation of the evolution into an infinite set of differential equation in terms of a_n,

$$\mu\frac{d}{d\mu}a_n^{A,V,T}(\mu) = -\frac{\alpha_s(\mu)}{2\pi}\gamma_n^{A,V,T}a_n^{A,V,T}(\mu). \tag{E6}$$

Now the hard evolution can be readily solved in terms of the Gegenbauer coefficients a_n,

$$a_n^{A,V,T}(Q) = a_n^{A,V,T}(Q_0)\left(\frac{\alpha_s(Q)}{\alpha_s(Q_0)}\right)^{\frac{\gamma_n^{A,V,T}}{\beta_0}} \tag{E7}$$

with the anomalous dimension [59,73]

$$\gamma_n^A = C_F\left[-3+4\sum_{j=1}^{n+1}\frac{1}{j}-\frac{2}{(n+1)(n+2)}\right], \tag{E8}$$

$$\gamma_n^V = C_F\left[-3+4\sum_{j=1}^{n+1}\frac{1}{j}-\frac{2}{(n+1)(n+2)}\right], \tag{E9}$$

$$\gamma_n^T = C_F\left(-4+4\sum_{j=1}^{n+1}\frac{1}{j}\right), \tag{E10}$$

where $C_F = \frac{N_c^2-1}{2N_c}$,

$$\alpha_s(Q) = \frac{4\pi}{\beta_0\ln(\frac{Q^2}{\Lambda_{\rm QCD}^2})},$$

$$\beta_0 = \frac{11}{3}N_c - \frac{2}{3}n_f,$$

and $\Lambda_{\rm QCD} = 226$ MeV.

[1] G. R. Farrar and D. R. Jackson, Phys. Rev. Lett. **43**, 246 (1979).
[2] X. Ji, Phys. Rev. Lett. **110**, 262002 (2013).
[3] J.-H. Zhang, J.-W. Chen, X. Ji, L. Jin, and H.-W. Lin, Phys. Rev. D **95**, 094514 (2017).
[4] A. V. Radyushkin, Phys. Rev. D **95**, 056020 (2017).
[5] S.-i. Nam, Mod. Phys. Lett. A **32**, 1750218 (2017).
[6] M. C. Chu, J. M. Grandy, S. Huang, and J. W. Negele, Phys. Rev. D **49**, 6039 (1994).
[7] D. Diakonov and V. Y. Petrov, Nucl. Phys. **B272**, 457 (1986).
[8] E. V. Shuryak, Nucl. Phys. **B319**, 541 (1989).
[9] M. A. Nowak, J. J. M. Verbaarschot, and I. Zahed, Nucl. Phys. **B325**, 581 (1989).
[10] M. Kacir, M. Prakash, and I. Zahed, Acta Phys. Pol. B **30**, 287 (1999).
[11] T. Schäfer and E. V. Shuryak, Rev. Mod. Phys. **70**, 323 (1998).
[12] E. Shuryak and I. Zahed, Phys. Rev. D **107**, 034023 (2023).
[13] E. Shuryak and I. Zahed, Phys. Rev. D **107**, 034024 (2023).
[14] E. Shuryak and I. Zahed, Phys. Rev. D **107**, 034025 (2023).
[15] E. Shuryak and I. Zahed, Phys. Rev. D **107**, 034026 (2023).
[16] E. Shuryak and I. Zahed, Phys. Rev. D **107**, 034027 (2023).
[17] L. Chang, I. C. Cloet, J. J. Cobos-Martinez, C. D. Roberts, S. M. Schmidt, and P. C. Tandy, Phys. Rev. Lett. **110**, 132001 (2013).
[18] C. Chen, L. Chang, C. D. Roberts, S. Wan, and H.-S. Zong, Phys. Rev. D **93**, 074021 (2016).
[19] M. Ding, K. Raya, D. Binosi, L. Chang, C. D. Roberts, and S. M. Schmidt, Phys. Rev. D **101**, 054014 (2020).
[20] E. Ruiz Arriola and W. Broniowski, Phys. Rev. D **66**, 094016 (2002).
[21] A. E. Dorokhov, W. Broniowski, and E. Ruiz Arriola, Phys. Rev. D **84**, 074015 (2011).
[22] W. Broniowski and E. Ruiz Arriola, Phys. Lett. B **773**, 385 (2017).
[23] W. Broniowski and E. Ruiz Arriola, Proc. Sci. Hadron2017 (**2018**) 174 [arXiv:1711.09355].
[24] M. Praszalowicz and A. Rostworowski, arXiv:hep-ph/0205177.
[25] D. G. Dumm, S. Noguera, N. N. Scoccola, and S. Scopetta, Phys. Rev. D **89**, 054031 (2014).
[26] V. Y. Petrov and P. V. Pobylitsa, arXiv:hep-ph/9712203.
[27] V. Y. Petrov, M. V. Polyakov, R. Ruskov, C. Weiss, and K. Goeke, Phys. Rev. D **59**, 114018 (1999).
[28] A. E. Dorokhov, Nuovo Cimento A **109**, 391 (1996).
[29] A. E. Dorokhov and L. Tomio, arXiv:hep-ph/9803329.
[30] I. V. Anikin, A. E. Dorokhov, and L. Tomio, Phys. At. Nucl. **64**, 1329 (2001).
[31] A. E. Dorokhov and L. Tomio, Phys. Rev. D **62**, 014016 (2000).
[32] S.-i. Nam, H.-C. Kim, A. Hosaka, and M. M. Musakhanov, Phys. Rev. D **74**, 014019 (2006).
[33] A. V. Radyushkin, arXiv:hep-ph/9406237.
[34] S. J. Brodsky, F.-G. Cao, and G. F. de Teramond, Phys. Rev. D **84**, 033001 (2011).
[35] S. J. Brodsky, G. F. de Teramond, H. G. Dosch, and J. Erlich, Phys. Rep. **584**, 1 (2015).
[36] S. Jia and J. P. Vary, Phys. Rev. C **99**, 035206 (2019).
[37] J. Lan, C. Mondal, S. Jia, X. Zhao, and J. P. Vary, Phys. Rev. Lett. **122**, 172001 (2019).
[38] W.-Y. Liu, E. Shuryak, and I. Zahed, Phys. Rev. D **107**, 094024 (2023).
[39] P. Maris and P. C. Tandy, Phys. Rev. C **62**, 055204 (2000).
[40] P. T. P. Hutauruk, I. C. Cloet, and A. W. Thomas, Phys. Rev. C **94**, 035201 (2016).
[41] A. Faessler, T. Gutsche, M. A. Ivanov, V. E. Lyubovitskij, and P. Wang, Phys. Rev. D **68**, 014011 (2003).
[42] A. Bashir, L. Chang, I. C. Cloet, B. El-Bennich, Y.-X. Liu, C. D. Roberts, and P. C. Tandy, Commun. Theor. Phys. **58**, 79 (2012).
[43] M. Chen, Chin. Phys. C **45**, 123104 (2021).
[44] M. A. Ivanov, J. G. Körner, J. N. Pandya, P. Santorelli, N. R. Soni, and C.-T. Tran, Front. Phys. (Beijing) **14**, 64401 (2019).
[45] D. Ebert, R. N. Faustov, and V. O. Galkin, Phys. Lett. B **635**, 93 (2006).
[46] D. Ebert, R. N. Faustov, and V. O. Galkin, Eur. Phys. J. C **47**, 745 (2006).
[47] H.-M. Choi, Phys. Rev. D **75**, 073016 (2007).
[48] E. P. Biernat and W. Schweiger, Phys. Rev. C **89**, 055205 (2014).
[49] R. M. Moita, J. P. B. C. de Melo, K. Tsushima, and T. Frederico, Phys. Rev. D **104**, 096020 (2021).
[50] T. M. Aliev, A. Ozpineci, and M. Savci, Phys. Lett. B **678**, 470 (2009).
[51] J. P. B. C. De Melo, Phys. Lett. B **788**, 152 (2019).
[52] D. Melikhov and S. Simula, Phys. Rev. D **65**, 094043 (2002).
[53] W. Jaus, Phys. Rev. D **67**, 094010 (2003).
[54] A. I. Vainshtein, V. I. Zakharov, V. A. Novikov, and M. A. Shifman, Sov. Phys. Usp. **25**, 195 (1982).
[55] T. Schäfer, E. V. Shuryak, and J. J. M. Verbaarschot, Phys. Rev. D **51**, 1267 (1995).
[56] W. Bentz, T. Hama, T. Matsuki, and K. Yazaki, Nucl. Phys. **A651**, 143 (1999).
[57] K. Itakura and S. Maedan, Phys. Rev. D **62**, 105016 (2000).
[58] K. Naito, S. Maedan, and K. Itakura, Phys. Rev. D **70** (2004).
[59] A. Kock, Y. Liu, and I. Zahed, Phys. Rev. D **102**, 014039 (2020).
[60] A. Kock and I. Zahed, Phys. Rev. D **104**, 116028 (2021).
[61] K. Olive, Chin. Phys. C **38**, 090001 (2014).
[62] P. Faccioli and E. V. Shuryak, Phys. Rev. D **64**, 114020 (2001).
[63] D. Ebert and H. Reinhardt, Nucl. Phys. **B271**, 188 (1986).
[64] C. Schüren, F. Döring, E. Ruiz Arriola, and K. Goeke, Nucl. Phys. **A565**, 687 (1993).
[65] G. S. Bali, V. M. Braun, S. Bürger, M. Göckeler, M. Gruber, F. Hutzler, P. Korcyl, A. Schäfer, A. Sternbeck, and P. Wein (RQCD Collaboration), J. High Energy Phys. 08 (2019) 065; 11 (2020) 037(A).
[66] C. Shi, C. Chen, L. Chang, C. D. Roberts, S. M. Schmidt, and H.-S. Zong, Phys. Rev. D **92**, 014035 (2015).
[67] E. M. Aitala *et al.* (E791 Collaboration), Phys. Rev. Lett. **86**, 4768 (2001).
[68] W. Broniowski, E. R. Arriola, and K. Golec-Biernat, Phys. Rev. D **77**, 034023 (2008).

[69] R. S. Plant and M. C. Birse, Nucl. Phys. **A628**, 607 (1998).
[70] R. D. Bowler and M. C. Birse, Nucl. Phys. **A582**, 655 (1995).
[71] N. G. Stefanis and A. V. Pimikov, Nucl. Phys. **A945**, 248 (2016).
[72] P. A. Boyle, D. Brommel, M. A. Donnellan, J. M. Flynn, A. Juttner, and C. T. Sachrajda (RBC, UKQCD Collaborations), Proc. Sci. LATTICE2008 (**2008**) 165 [arXiv:0810.1669].
[73] V. M. Braun *et al.*, J. High Energy Phys. 04 (2017) 082.
[74] Q. Chang, X.-N. Li, X.-Q. Li, and F. Su, Chin. Phys. C **42**, 073102 (2018).
[75] P. Ball and V. M. Braun, Phys. Rev. D **54**, 2182 (1996).
[76] O. Cata and V. Mateu, Phys. Rev. D **77**, 116009 (2008).
[77] M. Tanabashi *et al.* (Particle Data Group), Phys. Rev. D **98**, 030001 (2018).
[78] M. E. Carrillo-Serrano, W. Bentz, I. C. Cloët, and A. W. Thomas, Phys. Rev. C **92**, 015212 (2015).
[79] P. L. Chung, F. Coester, B. D. Keister, and W. N. Polyzou, Phys. Rev. C **37**, 2000 (1988).
[80] H. B. O'Connell, B. C. Pearce, A. W. Thomas, and A. G. Williams, Prog. Part. Nucl. Phys. **39**, 201 (1997).
[81] G. M. Huber *et al.* (Jefferson Lab Collaboration), Phys. Rev. C **78**, 045203 (2008).
[82] C. J. Bebek, C. N. Brown, S. D. Holmes, R. V. Kline, F. M. Pipkin, S. Raither, L. K. Sisterson, A. Browman, K. M. Hanson, D. Larson, and A. Silverman, Phys. Rev. D **17**, 1693 (1978).
[83] V. A. Nesterenko and A. V. Radyushkin, Phys. Lett. B **115**, 410 (1982).
[84] X. Gao, N. Karthik, S. Mukherjee, P. Petreczky, S. Syritsyn, and Y. Zhao, Phys. Rev. D **104**, 114515 (2021).
[85] L. Chang, I. C. Cloët, C. D. Roberts, S. M. Schmidt, and P. C. Tandy, Phys. Rev. Lett. **111**, 141802 (2013).
[86] C. J. Shultz, J. J. Dudek, and R. G. Edwards, Phys. Rev. D **91**, 114501 (2015).
[87] J. P. B. C. de Melo and T. Frederico, Phys. Rev. C **55**, 2043 (1997).
[88] H.-M. Choi and C.-R. Ji, Phys. Rev. D **70**, 053015 (2004).
[89] H. L. L. Roberts, A. Bashir, L. X. Gutierrez-Guerrero, C. D. Roberts, and D. J. Wilson, Phys. Rev. C **83**, 065206 (2011).
[90] Z.-F. Cui, D. Binosi, C. D. Roberts, and S. M. Schmidt, Phys. Lett. B **822**, 136631 (2021).
[91] M. S. Bhagwat and P. Maris, Phys. Rev. C **77**, 025203 (2008).
[92] A. F. Krutov, R. G. Polezhaev, and V. E. Troitsky, Phys. Rev. D **93**, 036007 (2016).
[93] B. Owen, W. Kamleh, D. Leinweber, B. Menadue, and S. Mahbub, Phys. Rev. D **91**, 074503 (2015).
[94] M. Oertel, M. Buballa, and J. Wambach, Nucl. Phys. **A676**, 247 (2000).